

Age-of-Information-Aware Distributed Task Offloading and Resource Allocation in Mobile Edge Computing Networks

Minwoo Kim, Jonggyu Jang, *Member, IEEE*, Youngchol Choi, and Hyun Jong Yang, *Member, IEEE*

Abstract—The growth in artificial intelligence (AI) technology has attracted substantial interests in age-of-information (AoI)-aware task offloading of mobile edge computing (MEC)—namely, minimizing service latency. Additionally, the use of MEC systems poses an additional problem arising from limited battery resources of MDs. This paper tackles the pressing challenge of AoI-aware distributed task offloading optimization, where user association (UA), resource allocation (RA), full-task offloading, and battery of mobile devices (MDs) are jointly considered. In existing studies, joint optimization of overall task offloading and UA is seldom considered due to the complexity of combinatorial optimization problems, and in cases where it is considered, linear objective functions such as power consumption are adopted. Revolutionizing the realm of MEC, our objective includes all major components contributing to users' quality of experience, including AoI and energy consumption. To achieve this, we first formulate an NP-hard combinatorial problem, where the objective function comprises three elements: communication latency, computation latency, and battery usage. We derive a closed-form RA solution of the problem; next, we provide a distributed pricing-based UA solution. We simulate the proposed algorithm for various vision and language AI tasks. Our numerical results show that the proposed method Pareto-dominates baseline methods. More specifically, the results demonstrate that the proposed method can outperform baseline methods by **1.62 times smaller AoI** with **41.2% less energy consumption**.

Index Terms—Age of information, mobile edge computing, resource allocation, user association, task offloading, energy efficiency, delay minimization, edge AI.



1 INTRODUCTION

AS artificial intelligence (AI) technology advances and support for AI capabilities in mobile devices (MDs) continues to grow, the demand for AI functions in edge computing is anticipated to surge. We have already experienced the impact of readily available AI applications such as voice-activated virtual assistants, generative model-based applications, and autonomous driving systems. AI applications' high demand for computing power and energy poses a significant challenge for MDs, as they are limited in processing power and battery life. A viable solution to this problem is the implementation of *task offloading* using mobile edge computing (MEC), which entails shifting local tasks to a remote edge server. While this approach lightens the computational burden on MDs, it increases the communication demands of the network. For edge servers, this results in an overall increase in both computational and communication loads, leading to potential service delays. Such delays in MEC environments can degrade the quality of services such as age of information (AoI). To minimize the AoI of the data while maintaining sustainability of MEC system devices, it is essential to jointly consider communication, computation resources, and energy consumption. Addressing these concerns, especially in systems heavily

reliant on AI, introduces a set of novel challenges to be tackled in optimizing task offloading.

1.1 Challenges for Task Offloading in MEC Systems

1) The need for full offloading of AI tasks. In general, as mentioned in [13], full offloading problems can be relaxed to partial offloading problems, which simplifies discrete variables into differentiable continuous variables. Thus, in many previous studies, partial offloading techniques are widely used to solve complex problems [1], [3], [14]. However, since most AI tasks are unsuitable for partial offloading, MEC optimization for AI task offloading requires hard decisions rather than soft decisions. This constraint is a challenge when applying AI task offloading into complex scenarios.

2) Joint optimization of user association and resource allocation. The process of offloading local tasks in a MEC network is analogous to the conventional user association and resource allocation (UARA) problem commonly encountered in wireless networks. Typically, in a UARA scenario, a user equipment (UE) connects to a base station (BS), and resources such as bandwidth are allocated accordingly. In a MEC environment, particularly in dense or heterogeneous networks, multiple base stations are available for an MD to connect with. Similar to traditional UARA scenarios, each MD associates with an edge server (ES), receiving allocations of both computational and communication resources. However, in MEC systems, the diversity in computational capabilities of both local and edge devices, such as variations in floating point operations per second

M. Kim, J. Jang, and H. J. Yang are with Department of Electrical Engineering, Pohang University of Science and Technology (POSTECH), (email: {mwkim0210, jgjang, hyunyang}@postech.ac.kr). Y. Choi is with the Korea Research Institute of Ships and Ocean Engineering (KRISO), (email: yc-choi@kriso.re.kr). M. Kim and J. Jang equally contributed. The corresponding author is Hyun Jong Yang.

TABLE 1
Comparison of the Proposed Method and Previous Works

Novelty and Related Works		Ours	[1] (‘23)	[2] (‘23)	[3] (‘23)	[4] (‘23)	[5] (‘23)	[6] (‘22)	[7] (‘22)	[8] (‘22)	[9] (‘22)	[10] (‘22)	[11] (‘21)	[12] (‘20)
Architecture	Multi-Cell Networks	✓	✓	-	✓	✓	-	-	-	✓	✓	-	-	✓
	Multi-User Networks	✓	✓	✓	✓	✓	✓	✓	✓	✓	✓	✓	✓	✓
	User Association	✓	-	-	✓	✓	-	-	-	-	✓	-	-	✓
	Resource Allocation	✓	✓	✓	✓	✓	✓	✓	✓	✓	✓	✓	✓	✓
	Full Offloading	✓	-	✓	-	-	-	-	✓	-	-	✓	-	✓
Objective	Energy Efficiency	✓	✓	✓	✓	✓	✓	-	-	✓	-	-	✓	-
	Delay Minimization	✓	✓	✓	✓	✓	✓	✓	✓	✓	✓	✓	✓	-
Approach	Optimization	✓	-	-	✓	-	✓	✓	✓	✓	-	-	✓	-
	Lyapunov	-	-	✓	✓	✓	-	-	-	-	-	-	-	✓
	Deep Learning	-	✓	-	-	✓	-	-	-	-	✓	✓	-	-
Performance Analysis	Latency Minimization	✓	✓	✓	-	✓	✓	✓	-	✓	✓	✓	-	-
	Energy Consumption	✓	✓	✓	✓	✓	-	-	-	✓	-	-	✓	-
Theoretical Analysis	Convergence Analysis	✓	✓	✓	-	✓	✓	-	-	✓	✓	✓	✓	✓
	Upperbound Analysis	✓	-	-	-	✓	-	-	-	-	-	-	-	✓

(FLOPS), VRAM capacity, and the number of available cores at the ESs, adds complexity to the MEC scenario. Additionally, in edge computing networks, delays incur from both computation and communication stages. Therefore, a joint approach to user association (UA) and resource allocation (RA) is necessary to effectively address the implications of these dual factors.

3) Trade-off between AoI and energy consumption. In a MEC system, local devices have the option to offload tasks to an edge server or process them locally. In scenarios where the edge server is heavily loaded, local computation can be advantageous in terms of latency, despite its higher energy consumption. In such situations, it is essential to prioritize task offloading based on the remaining battery life to maintain network continuity. It becomes necessary to understand the relationship between the degree of prioritization and the resulting latency versus local energy consumption. One of the key challenges is to find a Pareto-optimal solution that balances these factors effectively.

Motivated by these complexities in MEC systems, we identify several crucial questions:

- How can the remaining battery life of mobile devices be factored into the strategy for task offloading?
- What constitutes the most effective optimization strategy for distributed UARA that takes into account both communication and computation latency?

Building on these questions, our paper focuses on the specific constraints inherent in MEC systems and formulates an optimization problem for UARA. We develop a novel optimization-based solution to address this challenge. To validate the effectiveness of our solution, we conduct simulations under conditions that closely mimic real-world scenarios. The results of these simulations show that our model outperforms other baseline models in terms of latency and energy efficiency, highlighting its potential applicability in practical MEC environments.

1.2 Summary of Our Contributions

To the best of the authors’ knowledge, our work represents the first attempt at optimizing the joint problem of UARA for communication and computation resources in the context of *distributed* AI task offloading. The contributions of our work are multifaceted and can be summarized as follows:

- We unveil a groundbreaking AI task offloading strategy, optimization UARA in a novel approach. This strategy not only i) prioritizes full-task offloading with a keen eye on the MD’s battery level but also ii) features a fully distributed optimization of load balancing.
- We take on the challenge of the mixed-integer combinatorial optimization problem, which has not been solved in previous studies. To solve the problem, we leverage a novel auxiliary variable-based relaxation technique that enables us to balance loads by a continuous variable, not a combinatorial one. The solution we derive facilitates distributed optimization while simultaneously lowering the execution complexity.
- We provide a thorough analysis of both *the convergence and the optimality* of the distributed optimization problem, offering insights into the efficacy of our method.
- Through experimental results, we demonstrate that the proposed scheme consumes at least 39.1% less energy, while achieving a reduction in latency by at least 1.98 times. Best results in each objective show 5.29 times reduction in latency and 64.0% reduction in energy consumption. These findings are supported by simulations in practical environments, incorporating various AI services and load scenarios.

2 RELATED WORKS

Recent studies related to UARA optimization of MEC networks are categorized into the following subsections, where key characteristics of some of these works are compared with our work in Table 1.

2.1 Conventional Offloading Approaches: Pricing-Based Approach

Several studies [15]–[20] have been proposed for service/load offloading in cellular networks, characterized by ultra-dense networks, massive MIMO networks, heterogeneous networks (HetNets), and cloud random access networks (C-RAN). In [21], the authors proposed a modern approach for network load balancing. The aim of the approach is distributed optimization of UARA in HetNets. In the work, the concept of pricing-based load balancing has been proposed for the first time, which enables distributed network optimization without any additional information exchange between ESs. However, such approach was limited

to an objective function, specifically proportional fairness, where an artistic formulation led to a pricing framework. For instance, in [22], a pricing-based UARA optimization is further extended to backhaul-limited cellular networks.

Following [21], recent works have solved general framework for various objective functions such as α -fairness [15]. However, to the best of the authors' knowledge, there has been no previous study using pricing-based optimization for average delay minimization as well as computing/communication offloading in MEC scenarios.

2.2 Task Offloading in MEC

Task offloading studies in MEC systems have mainly focused on interpreting the problem as a conventional offloading problem with additional constraints such as user mobility and limited battery. Typical solution methods include solving optimization problems [3], [5], [6], [11], [14], [23]–[28] to better optimize their objective, mainly task latency and energy consumption. Some researchers took a different approach and used Lyapunov optimization method to solve UARA problems in MEC system [2], [4], [12], [29]. The authors of [30] used both Karush-Kuhn-Tucker (KKT) methods and Lyapunov optimization method to solve their problem. Growing number of researchers are implementing deep learning techniques such as deep reinforcement learning (DRL) to optimize task offloading in MEC systems [1], [9], [10], [31]–[36], due to DRL's potential to calculate optimal policies with comparably low computational load compared to calculating heuristic solutions. Additionally, DRL may provide an optimal solutions in cases where other optimization methods can only yield sub-optimal solutions. In [4], researchers used DRL after applying conventional solving methods to find the optimal solution.

Properties unique to AI-native MEC systems include energy constraints on MDs and full task offloading. Many studies have considered energy of MDs as a constraint [2], [23]. The authors of [37] have shown the fundamental trade-off between the delay and resource used in computing. Few studies have regarded energy of MDs as their objective [4], [28], [36]. Full offloading of tasks has also been dealt with in previous research [2], [6], [31]. The authors of [28] proposed a partial offloading design and compared the sum-energy consumption performance with other full offloading schemes.

Yet, none of the research have focused on jointly optimizing UARA and energy consumption, while considering full offloading scenario. Considering all of the factors is a complicated problem, but is necessary for achieving a solution that can be implemented in real life. In this work, we find a new solution to delay-minimizing UARA pricing scheme for multi-cell, multi-user, and multi-resource MEC networks.

3 SYSTEM MODEL AND PROBLEM FORMULATION

In this section, we first introduce the system model overview embracing communication/computation modeling. Then, we provide a joint UARA optimization problem for prioritized task offloading.

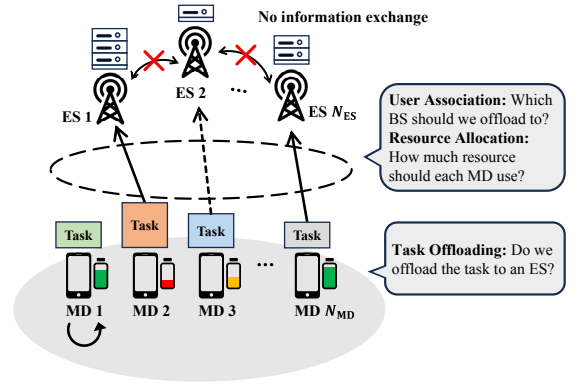


Fig. 1. An illustration of the system model. N_{MD} MDs with limited battery and heterogeneous tasks can associate with N_{ES} ESs. Information exchange between the ESs is unnecessary.

TABLE 2
Interpretation of the Notations Used in this Paper

Notation	Description
\mathcal{M}	Set of MDs
\mathcal{E}	Set of ESs
N_{MD}	Number of MDs
N_{ES}	Number of ESs
x_{ij}	Association indicator of MD i and ES j
y_{ij}	Frequency resource allocation ratio between MD i and ES j
z_{ij}	Computing resource allocation ratio between MD i and ES j
R_{ij}	Achievable data rate between MD i and ES j
d_i	Number of bits of the task generated by MD i
f_i	Number of flops required by MD i 's task
ρ_i	Ratio of task by MD i dependent on core count
B_i	Remaining battery of MD i
$D_{MD,i}$	Local computing delay of MD i
$D_{ES,i}$	Edge computing delay of MD i associated with ES j
G_i	Local computation penalty term of MD i
α	Balance coefficient between MD energy preservation and average latency

3.1 System Model Overview

Figure 1 illustrates a MEC network composed of N_{ES} edge servers and N_{MD} MDs, where each of the edge servers has its capacity-limited computing hardware. The total computation capacities of MD i and ES j are denoted as $F_{MD,i}$ and $F_{ES,j}$ respectively. We assume that each MD always has a task at hand, creating a task whenever the previous task is finished. The generated AI service at MD i has a computation load of f_i flops and a communication load of d_i bits. For readability, we summarize the variables used in this paper in Table 2.

In the edge server layer, each ES broadcasts its price to users in a decentralized manner. Based on the received prices, each MD aggregates load information from base stations to decide whether to compute locally or offload its task to a remote edge server. In this context, edge servers allocate

computing and communication resources to minimize the delay experienced by the users they are servicing.

Assumptions. In our system model, we have postulated the following assumptions to better emulate the real-world scenario and to ease the deployment of our proposed method.

- A1) We assume that the time intervals are small enough that the channel differences between adjacent time steps are negligible.
- A2) Based on the 3GPP small cell Scenario 1 [38], we assume all of the ESs share the cell areas, thereby cooperating to serve users efficiently.
- A3) We assume that the frequency reuse factor is N_{ES} , i.e., all the ESs occupy separate bandwidth.
 - As our objective is to optimize offloading over the long term, we can leverage the previous time step's channel interference to facilitate dynamic offloading and make full use of bandwidth resources.
- A4) For brevity of the notation, we omit the time step index in this paper. The index is negligible since our focus is on long-term optimization of network load balancing.

3.2 Task Offloading Variables and Constraints

In a MEC system, once a task is generated at an MD, the MD makes its offloading decision. Let x_{ij} denote the offloading decision of MD i regarding ES j . The association of MD i and ES j is represented by

$$x_{ij} = \begin{cases} 1, & \text{ES } j \text{ servers MD } i, \\ 0, & \text{otherwise.} \end{cases} \quad (1)$$

For readability, we define an augmented matrix of x_{ij} as $\mathbf{X} \in \{0, 1\}^{N_{MD} \times N_{ES}}$, where $[\mathbf{X}]_{i,j} = x_{ij}$. Since AI task cannot be partially offloaded, at most 1 ES can be associated to an MD. Hence, the UA indication variable x_{ij} is constrained as follows:

$$\sum_{k \in \mathcal{E}} x_{ik} \leq 1 \text{ and } x_{ij} \in \{0, 1\}, \forall i \in \mathcal{M}, j \in \mathcal{E}. \quad (2)$$

If $x_{ij} = 0$ for all $j \in \mathcal{E}$, MD i processes its task locally.

3.3 Communication Model

In this paper, we assume a flat power spectral density (PSD), i.e., the transmission power is uniform across all frequency resources for every MDs. The MDs transmit the task data with full transmission power, where the transmission power of MD i is denoted by P_i . To mitigate the inter-cell interference, the bandwidth is equally divided and occupied by different edge servers. Let us define the bandwidth of the network as W . Then, the total bandwidth of ES j is expressed as $W_j = W/B$, for all $j \in \mathcal{E}$. The allocated bandwidth is then divided and allocated to the associated MDs. The fraction of the bandwidth allocated from ES j to MD i is denoted by y_{ij} , i.e., the bandwidth allocated to MD i can be represented by $\sum_{j \in \mathcal{E}} y_{ij} W_j$.

To simplify our notation, we augment the variables y_{ij} to create \mathbf{Y} . Since the bandwidth allocated to each MD cannot overlap, the variable \mathbf{Y} is constrained by

$$\sum_{k \in \mathcal{M}} y_{kj} \leq 1 \text{ and } y_{ij} \in [0, 1], \forall i \in \mathcal{M}, j \in \mathcal{E}. \quad (3)$$

Capacity Model. Let h_{ij} denote the channel coefficient between MD i and ES j . Again, the allocated bandwidth of each MD does not overlap. We can therefore define the signal-to-noise-ratio (SNR) of MD i served by ES j as $\text{SNR}_{ij} = \frac{|h_{ij}|^2 P_i}{N_0}$.

Remark 1 (Interference model). Here, we operate under the assumption that the ES divides the bandwidth equally, which may not be optimal in terms of frequency efficiency. Nevertheless, by finely segmenting the time slots as previously designed, the interference state from the previous time slot approximates that of the current time slot. This allows for a distributed formulation of the Signal-to-Interference-plus-Noise Ratio (SINR) model, where the ESs share the total bandwidth.

Then, the achievable rate of MD i associated to an ES is defined by

$$\sum_{j \in \mathcal{E}} x_{ij} y_{ij} R_{ij}, \quad (4)$$

where the spectral efficiency R_{ij} is defined as

$$W_j \log(1 + \text{SNR}_{ij}). \quad (5)$$

Age of Information Injected from Communication. AoI is an important measure for many AI tasks, especially when they require real-time computation. In our scenario, AoI is incurred by 2 major components: communication latency and computation latency. Here, we examine the communication latency model. If an MD decides to process its task locally, there exists no communication delay. On the other hand, once an MD decides to offload a task to ES j , d_i bits of data should be transferred to ES j via a wireless channel before the service is processed.

Using the achievable rate definition in (4), we have the communication delay of MD i associated to ES j as follows:

$$\sum_{j \in \mathcal{E}} \frac{d_i x_{ij}}{R_{ij} y_{ij} + \epsilon} = \sum_{j \in \mathcal{E}} x_{ij} D_{\text{cm},ij}, \quad (6)$$

where an arbitrarily small constant ϵ is added to the denominator as a regularization technique to prevent potential computational issues associated with division by zero.

3.4 Computing Model

Here, we introduce our computing model and provide computing delay of local computation and edge computation. In general, local devices such as mobile devices and laptops have fewer computation cores compared to the ES (GPU server). For a more practical modeling of computing delay, we divide the computation of AI tasks into parallelizable and non-parallelizable parts. Since our objective is to minimize end-to-end delay, if parallelizable portion is high, offloading can lead to higher delay reduction due to abundant number of processors at the edge server. To model this delay model, we adopt Amdahl's law. Amdahl's law describes the relationship between the latency of a task and the number of available processors, accounting for the portion of the task where parallel computing is feasible:

$$\text{Amdahl's law: } S_{\text{latency}}(s) = \frac{1}{(1 - \rho) + \frac{\rho}{s}}, \quad (7)$$

where S_{latency} signifies the acceleration in completing the entire task, ρ represents the parallelizable fraction of the original task, and s denotes the achievable acceleration of the parallelizable proportion.

Computing Latency at MDs. If MD i has a computational task at hand, it can fully leverage its computing resource to the task. The total number of computing cores at MD i is represented as Z_{MD_i} , and each of the cores has a computing capacity of F_{MD_i} . From our assumption, up to one task is processed at an MD. Thus, the computing delay of MD i with task that requires f_i flops and has a parallelizable fraction of ρ_i is represented by

$$D_{\text{MD},i} = \frac{f_i}{F_{\text{MD}_i}}(1 - \rho_i) + \frac{f_i}{F_{\text{MD}_i}Z_{\text{MD}_i}}(\rho_i), \quad (8)$$

where the first term represents the delay obtained from the core-independent part of the task, and the second term represents the delay deriving from the parallelizable portion of the task.

Computing Latency at Edge Servers. The most significant difference in computation delay between local computing and task offloading is on shared computing resources. More simply, in each ES, the tasks offloaded from its associated MDs are simultaneously processed. Let $Z_{\text{ES},j}$ denote the total number of cores available at ES j . Then, if ES j allocates a fraction z_{ij} of computing cores to i , the task generated at MD i is computed with $Z_{\text{ES},j}z_{ij}$ cores. Thus, the computing delay of the task generated at MD i offloaded to ES j can be represented by

$$\sum_{j \in \mathcal{E}} \left(\frac{f_i}{F_{\text{ES},j} + \epsilon}(1 - \rho_i) + \frac{f_i}{F_{\text{ES},j}Z_{\text{ES},j}z_{ij} + \epsilon}\rho_i \right) x_{ij} \quad (9)$$

$$= \sum_{j \in \mathcal{E}} x_{ij} (D_{\text{ES}(s),ij} + D_{\text{ES}(p),ij}) \quad (10)$$

$$= \sum_{j \in \mathcal{E}} x_{ij} D_{\text{ES},ij}. \quad (11)$$

Similar to equation (6), a very small constant ϵ is added to the denominator to prevent indeterminacy occurring from division by zero. Also, the computing resource variable z_{ij} is constrained by

$$\sum_{k \in \mathcal{M}} z_{kj} \leq 1 \text{ and } z_{ij} \in [0, 1], \forall i \in \mathcal{M}, j \in \mathcal{E}. \quad (12)$$

Memory Requirement. Another factor to consider is the amount of memory the task consumes. The memory the tasks use should not exceed the VRAM of the edge device. If we denote the proportion of the memory used to load model parameter as M_j , the constraints imposed on the variable can be expressed as

$$\sum_{k \in \mathcal{M}} m_i x_{kj} \leq 1 - M_j, \forall i \in \mathcal{M}, j \in \mathcal{E}, \quad (13)$$

where m_i is the linearly-increasing memory consumption term.

Remark 2. When assessing the memory usage of AI models, both the number of parameters of the model and the number of activations should be examined. Here, we employ a model size computation method introduced in

[39] to calculate the memory size of Transformer-based models. The memory calculating equation is as follows:

$$\text{Memory} = p \times (sbhL(10 + \frac{24}{t} + 5\frac{as}{ht}) + |\theta|), \quad (14)$$

where p is the precision in bytes, s is the sequence length, b is the batch size, h is the size of the hidden dimension, L is the number of transformer layers, t is the tensor parallel size, a is the number of attention heads, and $|\theta|$ is the number of parameters of the model. We use this formula to assess the memory size of the AI models based on Vision Transformer (ViT).

3.5 Energy Consumption Model

Energy consumption at MDs. Most MDs have limited battery capacity while some user devices may be powered and therefore does not have finite battery capacity. To take this scenario into account and generalize our scenario, we compose our user set \mathcal{M} with both type of users, one with limited battery and the other with infinite energy.

In MDs, energy is expended on communication and computation. If a task is not offloaded, the device energy is spent on computation only. However, if offloading occurs, energy is expended on the transmission of radio waves at a specific frequency. We first look at the case of local computation. Let us define the computing energy efficiency as $\delta_{\text{cp},i}$ (Watt/flops). Then, the computing energy of MD i per unit time is represented by

$$E_{\text{cp},i} = \delta_{\text{cp},i} \cdot (F_{\text{MD}_i}(1 - \rho_i) + F_{\text{MD}_i}Z_{\text{MD}_i}\rho_i)(1 - \sum_{j \in \mathcal{E}} x_{ij}). \quad (15)$$

Next, defining the power efficiency of transmission of MD i as $\delta_{\text{cm},i}$, the energy consumption of MD i connected to ES j for offloading can be expressed as follows:

$$E_{\text{cm},i} = \delta_{\text{cm},i} \sum_{j \in \mathcal{E}} (x_{ij}y_{ij}W_j) P_i. \quad (16)$$

Thus, the total energy consumption at MD i is denoted by

$$E_{\text{tot},i} = E_{\text{cp},i} + E_{\text{cm},i} + E_{b,i}, \quad (17)$$

where $E_{b,i}$ denotes the base energy consumption required to operate MD i .

Energy consumption at Edge Servers. In ESs, the majority of the energy consumption is due to the computing process. Similar to equation (10), the total energy consumption required to process the offloaded tasks from MDs is denoted as

$$E_{\text{tot},j} = \delta_{\text{cp},j} \sum_{i \in \mathcal{M}} (F_{\text{ES},j}(1 - \rho_i) + F_{\text{ES},j}Z_{\text{ES},j}z_{ij}\rho_i), \quad (18)$$

where we omit the base energy consumption for brevity.

3.6 Problem Formulation

We first introduce the objective function of our problem formulation. We aim to minimize end-to-end delay while reducing energy consumption of low-battery-level MDs. Thus, the objective function is formulated by a balanced form of average end-to-end delay and battery usage.

Average Delay. Here, for brevity of the notation, we use sum-delay of the tasks generated from MDs as follows:

$$\begin{aligned} & \sum_{i \in \mathcal{M}} \sum_{j \in \mathcal{E}} x_{ij} (D_{\text{cm},ij} + D_{\text{ES},ij}) \\ & + \sum_{i \in \mathcal{M}} \left(1 - \sum_{j \in \mathcal{E}} x_{ij} \right) D_{\text{MD},i}. \end{aligned} \quad (19)$$

Penalized Term for Battery Usage for Low-Battery level MDs. We now formulate the energy consumption of local computation. The energy penalty of local processing is denoted as

$$G_i = \delta_{\text{cp},i} f_i - \delta_{\text{cm},i} \frac{d_i}{R_{ij}}. \quad (20)$$

Then, the energy consumption part of the objective function is formulated by

$$\max_{\mathbf{X}} \sum_{i \in \mathcal{M}} \left(1 - \sum_{j \in \mathcal{E}} x_{ij} \right) \frac{G_i}{B_i}, \quad (21)$$

where B_i is the remaining battery of MD i . We take the fractional representation of the two variables to enhance the consideration of device energy, particularly in situations where the energy levels are low.

By combining the objective functions (20) and (21) with the constraints presented in the previous sections, the UARA optimization problem is formulated as

$$\begin{aligned} \mathcal{P}_1: \min_{\mathbf{X}, \mathbf{Y}, \mathbf{Z}} & \sum_{i \in \mathcal{M}} \sum_{j \in \mathcal{E}} x_{ij} (D_{\text{cm},ij} + D_{\text{ES},ij}) \\ & + \sum_{i \in \mathcal{M}} \left(1 - \sum_{j \in \mathcal{E}} x_{ij} \right) \left(D_{\text{MD},i} - \alpha \frac{G_i}{B_i} \right) \quad (\mathcal{P}_1\text{a}) \\ \text{s.t.} & \quad (2) - (16), \quad (\mathcal{P}_1\text{b}) \end{aligned}$$

where α is the balance coefficient between MD energy preservation and average latency. In our problem, we do not incorporate energy conservation of ESs as an objective for minimization, given that each ES is typically connected to an energy source. Consequently, we prioritize on energy conservation of MDs with the risk of battery depletion due to limited battery capacity.

In Problem \mathcal{P}_1 , the main challenge is that the problem is in a non-linear form in terms of all unknown variables \mathbf{X} , \mathbf{Y} and \mathbf{Z} . Also, the binary variable \mathbf{X} is a combinatorial variable, coupled with \mathbf{Y} , which is continuous. This exacerbates the problem, as the problem becomes non-linear and a mixed-integer problem.

4 OPTIMIZATION-BASED OFFLOADING SCHEME

In this section, we propose a distributed task offloading framework via UARA optimization under MEC networks. To this end, we first solve the RA part of the original problem \mathcal{P}_1 for given UA variable \mathbf{X} , where closed-form solutions are obtained for both communication and computing RA variable. Next, we obtain the UA solution \mathbf{X} for the optimal \mathbf{Y} and \mathbf{Z} . The resulting solution minimizes the objective function, which is a balanced function of average latency and energy preservation. Furthermore, we analyze

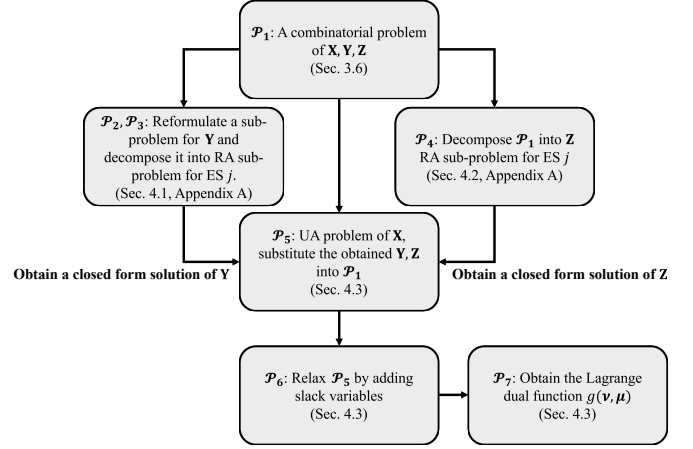


Fig. 2. Schematic of the algorithms for the latency and energy consumption minimization problem in the MEC system.

the optimality and convergence of the proposed algorithm in the next section.

4.1 Communication Resource Allocation With Fixed User Association

We first focus on solving for the variable \mathbf{Y} in the context of Problem \mathcal{P}_1 . For brevity of the explanation, we formulate a sub-problem, in which the other variables (\mathbf{X} and \mathbf{Z}) are fixed¹. Hence, Problem \mathcal{P}_1 can be reformulated to a subproblem for \mathbf{Y} as

$$\mathcal{P}_2: \min_{\mathbf{Y}} \sum_{i \in \mathcal{M}} \sum_{j \in \mathcal{E}} \frac{d_i x_{ij}}{R_{ij} y_{ij} + \epsilon} \quad (\mathcal{P}_2\text{a})$$

$$\text{s.t.} \quad \sum_{k \in \mathcal{M}} y_{kj} \leq 1, \quad \forall j \in \mathcal{E} \quad (\mathcal{P}_2\text{b})$$

$$y_{ij} \geq 0, \quad \forall (i, j) \in \mathcal{M} \times \mathcal{E}. \quad (\mathcal{P}_2\text{c})$$

Since all the constraints and objective function in Problem \mathcal{P}_2 are decomposable for each ES j , we can relax the problem into sub-problems for each ES j as follows:

$$\mathcal{P}_3: \min_{\mathbf{Y}} \sum_{i \in \mathcal{M}_j} \frac{d_i}{R_{ij} y_{ij}} \quad (\mathcal{P}_3\text{a})$$

$$\text{s.t.} \quad \sum_{k \in \mathcal{M}_j} y_{kj} \leq 1 \quad (\mathcal{P}_3\text{b})$$

$$y_{ij} \geq 0, \quad \forall i \in \mathcal{M}_j, \quad (\mathcal{P}_3\text{c})$$

where \mathcal{M}_j is a subset of \mathcal{M} such that $\mathcal{M}_j = \{i \in \mathcal{M} | x_{ij} = 1\}$.

We obtain the solution to the Problem \mathcal{P}_3 using the Karush-Kuhn-Tucker (KKT) conditions. For brevity of the notation, we present the details of the derivation in Appendix A.1, which can be found in the supplemental ma-

1. Here, although the variables \mathbf{X} and \mathbf{Z} are fixed, we can obtain a closed-form solution of \mathbf{Y} . That is to say, we can plug-in the optimal variable \mathbf{Y} into Problem \mathcal{P}_1 and solve the problem only for the variable \mathbf{X} . Furthermore, the variable \mathbf{Z} is independent with the variable \mathbf{Y} for fixed \mathbf{X} .

terial. From the solution of Problem \mathcal{P}_3 , the optimal bandwidth allocation is given as

$$y_{ij} = \left(\sqrt{d_i/R_{ij}} \right) / \left(\sum_{k \in \mathcal{M}_j} \sqrt{d_k/R_{kj}} \right) \quad (\mathcal{P}_2)$$

$$= \left(\sqrt{d_i/R_{ij}} \right) / \left(\sum_{k \in \mathcal{M}} \sqrt{d_k/R_{kj}x_{kj}} \right). \quad (\mathcal{P}_3)$$

4.2 Computing Resource Allocation With Fixed User Association

Similar to the bandwidth resource allocation from the previous section, the computing resource allocation problem can be decomposed for each ES j . The decomposed computing resource allocation sub-problem for ES j is represented by

$$\mathcal{P}_4: \min_{\mathbf{Z}} \sum_{i \in \mathcal{M}_j} \left(\frac{f_i(1-\rho_i)}{F_{ES,j}} + \frac{f_i\rho_i}{F_{ES,j}Z_{ES,j}z_{ij}} \right) \quad (\mathcal{P}_4a)$$

$$\text{s.t.} \quad \sum_{k \in \mathcal{M}_j} z_{kj} \leq 1 \quad (\mathcal{P}_4b)$$

$$z_{ij} \geq 0, \quad \forall i \in \mathcal{M}_j. \quad (\mathcal{P}_4c)$$

We use KKT conditions to find the optimal solution to Problem \mathcal{P}_4 . We omit the solution in this section, and we elaborate the solution in Appendix A.1 (available at the supplemental material). The optimal solution for the computing resource allocation is denoted as follows:

$$z_{ij} = \sqrt{\frac{f_i\rho_i}{F_{ES,j}Z_{ES,j}}} / \left(\sum_{k \in \mathcal{M}} \sqrt{\frac{f_k\rho_k}{F_{ES,j}Z_{ES,j}}} x_{kj} \right). \quad (\mathcal{P}_4d)$$

4.3 User Association

In Sections 4.1 and 4.2, we obtain the optimal solutions of \mathbf{Y} and \mathbf{Z} for given UA variable \mathbf{X} . Here, we aim to solve the optimization problem \mathcal{P}_1 , with the solutions for RA variables \mathbf{Y} and \mathbf{Z} are provided in (22) and (24), respectively.

First, for the brevity of the notation, we rewrite the problem \mathcal{P}_1 by substituting the optimal RA solutions into the problem. The problem can be reformulated as

$$\mathcal{P}_5: \min_{\mathbf{X}} \sum_{j \in \mathcal{E}} \left(\sum_{i \in \mathcal{M}} \sqrt{D_{ES(s),ij}x_{ij}} \right)^2 + \sum_{j \in \mathcal{E}} \left(\sum_{i \in \mathcal{M}} \sqrt{D_{cm,ij}x_{ij}} \right)^2 + \sum_{j \in \mathcal{E}} \sum_{i \in \mathcal{M}} c_{ij}x_{ij} \quad (\mathcal{P}_5a)$$

$$\text{s.t.} \quad \sum_{j \in \mathcal{E}} x_{ij} \leq 1, \quad \forall i \in \mathcal{M} \quad (\mathcal{P}_5b)$$

$$x_{ij} \in \{0, 1\}, \quad \forall (i, j) \in \mathcal{M} \times \mathcal{E}, \quad (\mathcal{P}_5c)$$

where $c_{ij} = -D_{ES(p),ij} - D_{MD,i} + \alpha \frac{G_i}{B_i}$.

A well-designed heuristic method could also obtain a near-optimal solution; however, it would require heavy information exchange between the MDs in order to achieve good performance. As for our scheme, we show that an optimal solution is obtainable without such communication overhead.

Before solving the problem; the challenge is that the first and second terms in Equation (\mathcal{P}_5a) are non-linear to the binary variable x_{ij} and cannot be decomposed. To obtain solution, we may require computation-intensive exhaustive search, the computational complexity of which is $\mathcal{O}(N_{ES}^{N_{MD}+1}N_{MD})$. To resolve this issue, we propose a method to add two slack variables: i) $a_j = (\sum_{i \in \mathcal{M}} \sqrt{D_{cm,ij}x_{ij}})^2$ and ii) $b_j = (\sum_{i \in \mathcal{M}} \sqrt{D_{ES(s),ij}x_{ij}})^2$, where $\mathbf{a} = [a_1, \dots, a_{N_{ES}}]$ and $\mathbf{b} = [b_1, \dots, b_{N_{ES}}]$. With these slack variables, we can reformulate the problem \mathcal{P}_5 without loss of generality, as follows:

$$\mathcal{P}_6: \min_{\mathbf{a}, \mathbf{b}, \mathbf{X}} \sum_{j \in \mathcal{E}} (a_j + b_j) + \sum_{i \in \mathcal{M}} \sum_{j \in \mathcal{E}} c_{ij}x_{ij} \quad (\mathcal{P}_6a)$$

$$\text{s.t.} \quad \sum_{j \in \mathcal{E}} x_{ij} \leq 1, \quad \forall i \in \mathcal{M} \quad (\mathcal{P}_6b)$$

$$x_{ij} \in \{0, 1\}, \quad \forall (i, j) \in \mathcal{M} \times \mathcal{E} \quad (\mathcal{P}_6c)$$

$$\sqrt{a_j} = \sum_{i \in \mathcal{M}} \sqrt{D_{cm,ij}x_{ij}} \quad (\mathcal{P}_6d)$$

$$\sqrt{b_j} = \sum_{i \in \mathcal{M}} \sqrt{D_{ES(s),ij}x_{ij}}. \quad (\mathcal{P}_6e)$$

Now, the objective function of the problem given by (\mathcal{P}_6a) is linear. Furthermore, x_{ij} related terms in the constraints are all linear, which enables us to find the optimum \mathbf{X} by minimizing the Lagrangian of problem \mathcal{P}_6 . Interestingly, the association variable x_{ij} of MD i can be computed in MD i locally without exchanging information with other MDs. Henceforth, in Lagrangian duality approach, if the Lagrangian multiplier of the dual problem can be computed distributedly, the algorithm can be implemented in a fully distributed manner. In the remainder of this section, we solve the problem in the following steps:

- 1) Minimization of Lagrangian of Problem \mathcal{P}_6 with respect to variables \mathbf{X} , \mathbf{a} , and \mathbf{b} . ($\mathcal{L}(\mathbf{X}, \mathbf{a}, \mathbf{b})$.)
- 2) Obtain dual objective function $g(\boldsymbol{\mu}, \boldsymbol{\nu})$ of Problem \mathcal{P}_6 by substituting the optimal variables (from step 1) into the problem.
- 3) Solve the Lagrangian dual function by maximizing the dual objective function.

4.3.1 Step 1: Minimize Lagrangian

In the first step of the Lagrangian duality approach, we obtain the Lagrangian dual objective function of the problem \mathcal{P}_6 . To this end, we formulate problem \mathcal{P}_6 into the Lagrangian form as follows:

$$\begin{aligned} \mathcal{L}(\mathbf{X}, \mathbf{a}, \mathbf{b}) = & \sum_{j \in \mathcal{E}} (a_j + b_j) + \sum_{i \in \mathcal{M}} \sum_{j \in \mathcal{E}} c_{ij}x_{ij} \\ & + \sum_{j \in \mathcal{E}} \mu_j \left(-\sqrt{a_j} + \sum_i \sqrt{D_{cm,ij}x_{ij}} \right) \\ & + \sum_{j \in \mathcal{E}} \nu_j \left(-\sqrt{b_j} + \sum_i \sqrt{D_{ES(s),ij}x_{ij}} \right), \end{aligned} \quad (25)$$

where μ_j and ν_j are the Lagrangian multipliers corresponding to the constraints (\mathcal{P}_6d) and (\mathcal{P}_6e). For simplicity, we define augmented vector notation of Lagrangian multipliers

by $\boldsymbol{\mu} = [\mu_1, \dots, \mu_{N_{\text{ES}}}]$ and $\boldsymbol{\nu} = [\nu_1, \dots, \nu_{N_{\text{ES}}}]$. We can now obtain the Lagrangian dual objective function by

$$g(\boldsymbol{\mu}, \boldsymbol{\nu}) = \min_{\mathbf{X}, \mathbf{a}, \mathbf{b}} \mathcal{L}(\mathbf{X}, \mathbf{a}, \mathbf{b}). \quad (26)$$

Because the primal variables \mathbf{a} , \mathbf{b} , and \mathbf{X} in Lagrangian are not coupled, we minimize those variables separately.

Step 1-1: Minimizers \mathbf{a}^* and \mathbf{b}^* for Lagrangian. Because the Lagrangian (25) is strongly convex, the minimizers \mathbf{a} and \mathbf{b} can be obtained by first-order optimality condition. Denoting the minimizers by $\mathbf{a}^* = [a_1^*, \dots, a_{N_{\text{ES}}}^*]$ and $\mathbf{b}^* = [b_1^*, \dots, b_{N_{\text{ES}}}^*]$, we have the following condition:

$$\frac{\partial \mathcal{L}}{\partial a_j} = 1 - \frac{\mu_j}{2\sqrt{a_j}} = 0 \implies a_j^* = \frac{\mu_j^2}{4} \quad (27)$$

$$\frac{\partial \mathcal{L}}{\partial b_j} = 1 - \frac{\nu_j}{2\sqrt{b_j}} = 0 \implies b_j^* = \frac{\nu_j^2}{4}. \quad (28)$$

Step 1-2: Minimizer \mathbf{X}^* for Lagrangian. Let us define the optimal \mathbf{X} minimizing Lagrangian \mathcal{L} as \mathbf{X}^* . Although the variable \mathbf{X} is combinatorial, the minimizer \mathbf{X}^* for the Lagrangian can be easily obtained since $x_{ij} \in \{0, 1\}$ and $\sum_{j \in \mathcal{E}} x_{ij} \leq 1$. More specifically, \mathbf{X}^* can be obtained by selecting index j (ES j) with the minimum coefficient, whereas none of the ESs are chosen if the minimum coefficient is larger than zero, i.e.,

$$x_{ij}^* = \begin{cases} 1, & j = \operatorname{argmin}(\mu_j \sqrt{D_{\text{cm}, ij}} + \nu_j \sqrt{D_{\text{ES}(s), ij}} \\ & + c_{ij}), \\ 0, & \text{otherwise.} \end{cases} \quad (29)$$

4.3.2 Step 2: Formulate Lagrangian dual problem

Substituting the minimizers \mathbf{X}^* , \mathbf{a}^* , and \mathbf{b}^* into the Lagrangian, we rewrite the Lagrangian dual objective function of (26) as

$$g(\boldsymbol{\mu}, \boldsymbol{\nu}) = - \sum_{j \in \mathcal{E}} \left(\frac{\mu_j^2}{4} + \frac{\nu_j^2}{4} \right) + \sum_{i \in \mathcal{M}} \min_{j \in \mathcal{E}} (\mu_j \sqrt{D_{\text{cm}, ij}} + \nu_j \sqrt{D_{\text{ES}(s), ij}} + c_{ij}). \quad (30)$$

Since the minimum of affine functions is concave, the new dual objective function (30) is a concave function. Finally, we find the optimum $\boldsymbol{\mu}$ and $\boldsymbol{\nu}$ by maximizing the Lagrangian dual objective function as follows:

$$\mathcal{P}_7: \max_{\boldsymbol{\mu}, \boldsymbol{\nu}} g(\boldsymbol{\mu}, \boldsymbol{\nu}). \quad (\mathcal{P}_7\text{a})$$

4.3.3 Step 3: Solve Lagrangian dual problem

In order to find the optimal solutions $\boldsymbol{\mu}^*$ and $\boldsymbol{\nu}^*$ of Problem \mathcal{P}_7 , we use the sub-gradient descent method, which is widely used in the optimization of non-differentiable functions. In fact, the dual function is sub-differentiable because the dual function $g(\boldsymbol{\mu}, \boldsymbol{\nu})$ is the minimum of affine functions of $\boldsymbol{\mu}$ and $\boldsymbol{\nu}$. Thus, we design the sub-gradient descent algorithm by

$$\begin{aligned} \mu_j &\leftarrow \mu_j + \eta_1 \left(\sum_{i \in \mathcal{M}} \sqrt{D_{\text{ES}(s), ij}} x_{ij}^* - \frac{\mu_j}{2} \right) \\ \nu_j &\leftarrow \nu_j + \eta_2 \left(\sum_{i \in \mathcal{M}} \sqrt{D_{\text{ES}(s), ij}} x_{ij}^* - \frac{\nu_j}{2} \right), \end{aligned} \quad (31)$$

Algorithm 1 Pricing-Based Distributed Task Offloading Algorithm for Latency Minimization

```

1: Initialisation:
2:   – Randomly initialize  $\nu_j$  and  $\mu_j$  for all  $j \in \mathcal{E}$ .
3:   – Initialize step size  $\eta_1$  and  $\eta_2$ .
4: for  $t = 0$  to  $T$  do
5:   ES  $j$  for all  $j \in \mathcal{E}$  broadcast prices  $\mu_j$  and  $\nu_j$  to users.
   ▷ Broadcast Price
6:   for  $i \in \mathcal{M}$  do
7:     if MD  $i$  generates a service then
8:       Update  $x_{ij}$ ,  $j \in \mathcal{E}$  by (29).   ▷ Task offloading
9:     end if
10:  end for
11:  for  $j \in \mathcal{E}$  do
12:    # Locally update the lines 13 - 15 at ES  $j$ 
13:    Update  $y_{ij}$  and  $z_{ij} \forall i \in \mathcal{M}_j$  by (22) and (24).
14:    Update  $\mu_j$  and  $\nu_j$  by (31).   ▷ Update price
15:  end for
16: end for

```

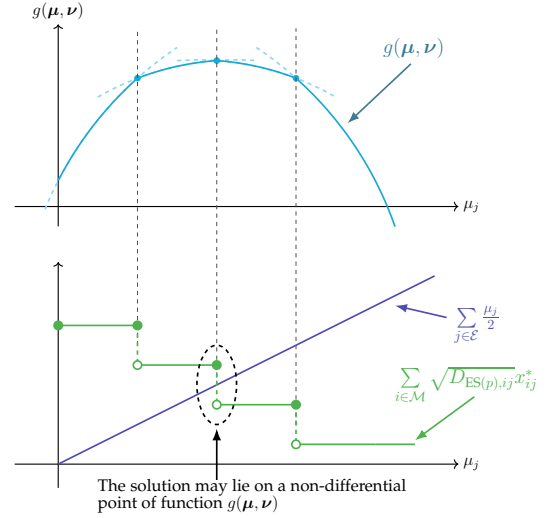


Fig. 3. Intuition of the situation that the solution lies on a non-differentiable point.

where η_1 and η_2 denote the step sizes for $\boldsymbol{\mu}$ and $\boldsymbol{\nu}$, respectively. As we mentioned before, the update procedure in (31) can be done with local information only; thus, the proposed method can optimize the load of the network in a distributed manner.

In Algorithm 1, we present a detailed step-by-step implementation of the proposed scheme.

5 OPTIMALITY AND CONVERGENCE ANALYSIS

In Section 4, we proposed a joint task offloading and resource allocation scheme for long-term delay minimization. The proposed method can be implemented in multiple edge servers without cooperation. In this section, we analyze the optimality and convergence of the proposed algorithm.

5.1 Optimality

From Sections 4.1 and 4.2, the RA solutions (22) and (24) are globally optimal for given \mathbf{X} . Therefore, there is no optimality loss in the RA solutions. However, in the optimization

of \mathbf{X} , there may exist a gap between the dual solution and primal solution. Here, we analyze the duality gap of the UA problem and the convergence of the proposed scheme.

Before analyzing the optimality, we clarify that the constraints on slack variables (\mathcal{P}_6d) and (\mathcal{P}_6e) may not be satisfied if \mathbf{X} is recovered by (29). Figure 3 illustrates the intuition that the solution cannot always satisfy the slack constraints. As depicted in the figure, the gradients of $g(\boldsymbol{\mu}, \boldsymbol{\nu})$ respect to $\boldsymbol{\mu}$ and $\boldsymbol{\nu}$ are represented by

$$\begin{aligned} \frac{\partial g}{\partial \mu_j} &= \sum_{i \in \mathcal{M}} \sqrt{D_{\text{ES}(s),ij} x_{ij}^*} - \frac{\mu_j}{2} \\ \frac{\partial g}{\partial \nu_j} &= \sum_{i \in \mathcal{M}} \sqrt{D_{\text{ES}(p),kj} x_{ij}^*} - \frac{\nu_j}{2}. \end{aligned} \quad (32)$$

Simply put, because the dual function g is concave, if the dual function is differentiable at all points, the solution must satisfy

$$\frac{\mu_j}{2} = \sum_{i \in \mathcal{M}} \sqrt{D_{\text{ES}(s),ij} x_{ij}^*} \text{ and } \frac{\nu_j}{2} = \sum_{i \in \mathcal{M}} \sqrt{D_{\text{ES}(p),kj} x_{ij}^*}. \quad (33)$$

The condition (33) is satisfied if the two terms, i) monotonically decreasing affine term and ii) monotonically increasing step-like term², are equal.

However, as depicted in Fig. 3, since \mathbf{X} is in a discrete space, the solution may lie on a non-differentiable point. The green-colored fist term is discontinuous at the points where the output of the argmin operator in (29) changes. That is, the objective function of Problem \mathcal{P}_7 can be non-differentiable for $\boldsymbol{\mu}$ or $\boldsymbol{\nu}$. The black dashed circle in Fig. 3 indicates an example where the solution is located at a non-differentiable point. This means that the constraints (\mathcal{P}_6d) and (\mathcal{P}_6e) cannot be satisfied. Whether the constraints (\mathcal{P}_6d) and (\mathcal{P}_6e) are satisfied or not, we can recover the variable \mathbf{X} using (29); however, the average latency term in the objective function of Problem \mathcal{P}_6 is different from the actual latency, as written below:

- The objective function of the primal problem \mathcal{P}_6 : $\sum_{j \in \mathcal{E}} (a_j + b_j) + \sum_{i \in \mathcal{M}} \sum_{j \in \mathcal{E}} c_{ij} x_{ij}$.
- Actual delay with penalized energy consumption corresponding to \mathbf{X} :

$$\begin{aligned} & \sum_{j \in \mathcal{E}} \left(\sum_{i \in \mathcal{M}} \sqrt{D_{\text{ES}(s),ij} x_{ij}} \right)^2 + \sum_{j \in \mathcal{E}} \left(\sum_{i \in \mathcal{M}} \sqrt{D_{\text{cm},ij} x_{ij}} \right)^2 \\ & + \sum_{i \in \mathcal{M}} \sum_{j \in \mathcal{E}} c_{ij} x_{ij}. \end{aligned}$$

Hereby, the query is that the solution may be no longer optimal for Problem \mathcal{P}_6 . In Theorem 1, it is shown that the gap between the obtained solution and the globally optimal solution is bounded.

Theorem 1 (Weak duality condition). Let us define the UA variable recovered by the dual solution to Problem \mathcal{P}_7 as $\hat{\mathbf{X}}$, $\hat{\mathbf{a}}$, and $\hat{\mathbf{b}}$. Then, the performance gap between the solution $\hat{\mathbf{X}}$ and the globally optimal solution is bounded by $\mathcal{O}\left(\left(\Delta_j^{(1)}\right)^2 + \left(\Delta_j^{(2)}\right)^2\right)$, where

2. As the value of $\nu_{1,j}$ increases, the indicator x_{ij} changes one to zero, i.e., the services are offloaded to other ESs.

TABLE 3
Simulation Settings

Parameters	Values	Parameters	Values
N_{MD}	20 to 160	N_{ES}	4 to 12
Bandwidth (MHz)	10	Maximum transmission power (dBm)	30
Noise power (dBm/Hz)	-174	Pathloss (dB)	$41 + 28 \log_{10}(d)$
δ_{sp}	10^9	α	0 to 100
$\delta_{\text{cm},i}$	2.6		

$$\Delta_j^{(1)} = \sqrt{a_j} - \left(\sum_{i \in \mathcal{M}} \sqrt{D_{\text{cm},ij} x_{kj}} \right) \text{ and } \Delta_j^{(2)} = \sqrt{b_j} - \left(\sum_{i \in \mathcal{M}} \sqrt{D_{\text{ES}(s),ij} x_{ij}} \right).$$

Proof: For the proof of the proposition, please consult Appendix B in the supplementary materials. \square

Extension to Machine Learning (L_2 Loss Minimization Approach). We have $a_j = \mu_j^2/4$ and $b_j = \nu_j^2/4$, where $a_j, b_j \geq 0$. In machine learning approaches for task offloading [15], the learning algorithm aims to minimize a loss function. If we set the loss function for minimizing the error terms as $\ell = \left(\Delta_j^{(1)}\right)^2 + \left(\Delta_j^{(2)}\right)^2$, we can rewrite the gradient descent step in (31) as follows:

$$\begin{aligned} \mu_j &\leftarrow \mu_j + \eta_1 \frac{\partial \ell}{\partial \mu_j} \\ \nu_j &\leftarrow \nu_j + \eta_2 \frac{\partial \ell}{\partial \nu_j}. \end{aligned} \quad (34)$$

5.2 Convergence Analysis

It is well known that the sub-gradient descent method generally converges to the optimal point if the problem is a convex function. Here, we show that the proposed scheme converges within $\mathcal{O}(1/\epsilon^2)$ gradient descent steps.

Proposition 1 (Convergence of the proposed scheme). Let us define the sequence of Lagrange multipliers $(\boldsymbol{\mu}, \boldsymbol{\nu})$ updated by (31) as $(\boldsymbol{\mu}^{(0)}, \boldsymbol{\nu}^{(0)})$, $(\boldsymbol{\mu}^{(1)}, \boldsymbol{\nu}^{(1)})$, ..., $(\boldsymbol{\mu}, \boldsymbol{\nu})$ for arbitrary k . We define the best solution until the T -th step as $g_{\max,k} = \max_{t=0,\dots,T} g(\boldsymbol{\mu}, \boldsymbol{\nu})$. Then, for any $\epsilon > 0$, there exist a constant step size (η_1, η_2) and optimization step $T \in \mathcal{O}(1/\epsilon^2)$ satisfying the following inequality:

$$g^* - g_{\max,T} \leq \epsilon, \quad (35)$$

where $g^* = \max_{\boldsymbol{\mu}, \boldsymbol{\nu}} g(\boldsymbol{\mu}, \boldsymbol{\nu})$.

Proof: The proof is shown in Appendix C, which is located in the supplementary material. \square

6 PERFORMANCE EVALUATION

In this section, we evaluate the proposed UARA offloading scheme in realistic AI-native MEC systems. Our scheme is tested and compared in diverse network scenarios. Our network scenarios include different network loads, different number of MDs and ESs and different simulation parameters. We first introduce our simulation environment in subsection 6.1, and show the performance of our scheme in subsection 6.2.

6.1 Simulation Environment

We use the 3GPP small cell simulation document to model our channel [38], [40]. The parameters are listed in detail in Table 3. The cell consists of two type of users: clustered users and uniformly distributed users. Clustered users typically increase the overall latency of the network, as the users in close proximity are more likely to be associated to the same ES. Still, clustered users are considered in order to better mimic the actual network scenarios. These different types of users allow us to simulate a more realistic cell network environment. Additionally, in order to reproduce a more task-intensive network, we prompt our users to generate tasks right after the completion of their previous tasks, which increases the chance of the network saturating.

The number of MDs ranges from 20 to 160. We use various types of MDs, including energy-limited mobile devices and energy-unlimited local computers. For energy-limited mobile devices, we use Samsung’s Galaxy S23, Huawei’s Mate 60, and Apple’s iPhone 14, some of the latest mobile devices available in the market. As for the energy-unlimited computers, we use Apple’s iMac with M1 processor. We use 4 to 12 number of ESs for our simulation. Each ES is equipped with computing resources that outperforms MD’s computing power. We use a combination of NVIDIA’s RTX 2080, RTX 3090 and A6000 as the ES’s computing device.

As for the tasks that the users generate, we use both the language-based AI tasks and computer vision tasks. Typically, large language models (LLMs) that deal with language tasks require large computing power and small input size. In contrast, computer vision models require comparably small computing resources, while the communication loads are relatively big due to larger input data. We combine these two tasks in different ratio. For language tasks, we employ Llama 2 model with approximately 7 billion parameters. As for vision tasks, we use a combination of convolutional neural network (CNN)-based models and ViT-based models. Specifically, we adopt 2 residual net (ResNet) models, 2 MobileNet models, ViT-based side adapter network (SAN) and pyramid scene parsing network (PSPNet). Using these tasks, we simulate three types of networks: network with high communication load, network with heavy computational load and a network with balanced load. In a network with high communication load, the tasks predominantly consist of vision tasks. The task parameters are listed in Table 4. The table values are based on the simulation results and calculations conducted by the authors. As for a network with high computational load, the tasks that the users generate is mainly comprised of language tasks.

We compare our results with some reference agents, which uses different policy schemes named as

- **Random scheme**, where the MDs choose the device (either one of N_{ES} ESs or locally) to compute randomly. The probability distribution of the selection follows a uniform distribution.
- **Max SINR scheme** [41], where the MDs determines which ES to associate based on the channel quality between the ESs and the device. The channel quality is assessed based on the uplink SINR. Hence, following this scheme, the MDs will achieve low communication delay.

TABLE 4
Communication and Computation Loads of the AI Tasks

Tasks	Communication [bits]	Computational [flops]
Llama (7 billion)	4.1×10^3	5.0×10^{13}
ResNet18	6.0×10^6	4.2×10^9
ResNet50	6.0×10^6	1.8×10^9
MobileNetV2	3.2×10^7	3.0×10^8
MobileNetV3	3.2×10^7	8.0×10^{12}
SAN	9.6×10^7	7.2×10^{13}
PSPNet	3.2×10^7	5.2×10^{13}

- **Max Compute scheme** [42], [43], which enables MDs to determine the computing device depending on the computational load on the ESs. Computing delay is a major component of the overall latency of the system, alongside communication delay. To devise a scheme that reduces the computational delay, we revise the approaches used in previous works [42], [43].
- **Combined scheme**, which is a mixture of the max SINR scheme and the max compute scheme. The MDs employing combined offloading scheme determine the computing device based on both the communication channel information and the computing resource information.

For all schemes, we allow the the MDs to compute their task locally with probability ϵ . This allows for fair comparison between the heuristic schemes and the proposed scheme, as the proposed scheme is allowed to compute locally. Enabling local computation also allows us to analyze the effects of local computation ratio. In our simulation, we use $\epsilon = 0.2$, as it leads to approximately uniform offloading between the ESs and the local device.

6.2 Evaluation Results

In this section, we conduct simulations to assess the effectiveness of our proposed model.

6.2.1 Latency Analysis

Figure 4 illustrates the latency of the proposed and the reference schemes with respect to the number of MDs, which ranges from 20 to 160. Our scheme is tested in three network scenarios: network with balanced load, communication-intensive network, and computational-intensive network. The simulation results show that for all network scenarios, the proposed achieves the lowest latency. More specifically, in a network with 160 MDs, the proposed scheme achieves 55.3%, 81.1%, and 64.7% lower latency compared to the best performing reference scheme in each of the network scenario. From the figures, we can see that the proposed scheme achieves a latency that is almost constant compared to the baseline schemes, which grow linearly. From Fig. 4b, which depicts the latency of the schemes in a network with high communication load, we observe that the max SINR scheme outperforms other baselines due to its performance in dealing with communication delay. However, it does not excel the performance of the proposed scheme. Fig. 4c shows the latency of the schemes in a computation-intensive network. Similar to Fig. 4b, max compute scheme achieves the

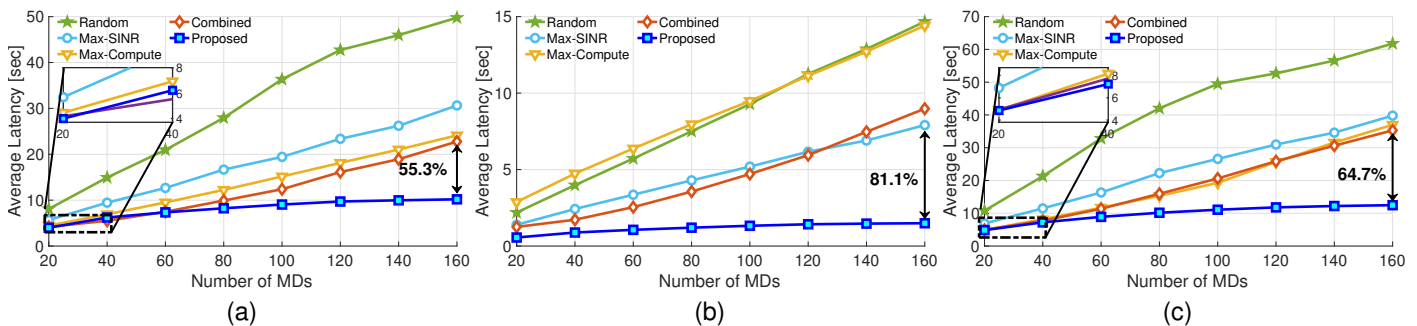


Fig. 4. The system latency under different network scenarios of a MEC network where $N_{ES} = 4$ and $\alpha = 1$: (a) Network with average communication and computational load; (b) High communication load network; (c) High computational load network.

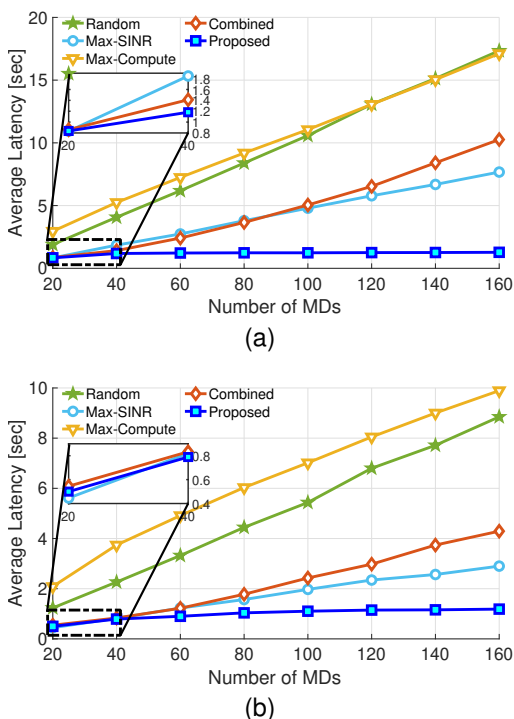


Fig. 5. Communication latency of networks with **high communication load**, where $\alpha = 1$: (a) Communication latency of a network with $N_{ES} = 4$; (b) Communication latency of a network with $N_{ES} = 8$.

lowest latency among the baseline schemes. Nonetheless, it still does not exceed the performance of the proposed scheme. The reason for the proposed scheme's exceptional performance is based on the simultaneous consideration of communication/computational latency and flexible offloading policy. How the proposed scheme outperforms other baselines is better illustrated in Figs. 5 and 6.

Figures 5 and 6 show the major latency component of different network scenarios as the number of users increases. Specifically, Fig. 5 illustrates the latency of users in a network with heavy communication load. As for the baseline schemes, the performance degrades severely as the available number of ESs decreases from 8 to 4. However, the proposed scheme maintains similar latency for all scenarios, showing that the algorithm is comparatively invariant to the amount of available resources. In a network with high communication load, the communication latency term becomes

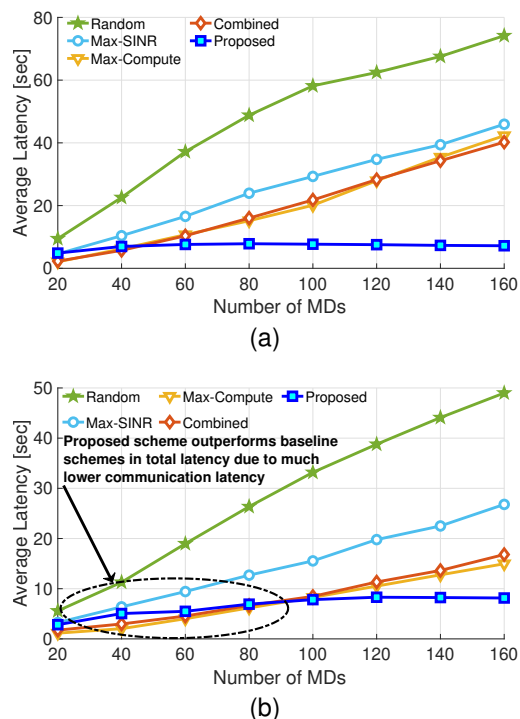


Fig. 6. Computational latency of networks with **high computation load**, where $\alpha = 1$: (a) Computational latency of a network with $N_{ES} = 4$; (b) Computational latency of a network with $N_{ES} = 8$.

the dominating factor in the overall latency of equation (19). Hence, the optimization process of the proposed method is focused on optimizing the communication latency. As a result, the proposed scheme achieves the lowest communication latency. Our method achieves latency lower than the max SINR method, which can be regarded as a theoretical short-term lower bound of the communication latency.

On the other hand, in a network experiencing heavy computational load (Fig. 6), our scheme dynamically focuses on reducing the computational latency. Similar to the communication-intensive network, this is due to the fact that computational delay is the dominating term of the latency formula.

The results indicate that the proposed scheme is able to achieve a low latency, regardless of the network environment. The proposed scheme outperforms other baseline schemes, even the schemes that specialized in specific net-

TABLE 5

Energy consumption per task of each scheme in different network environment with $N_{ES} = 12$. Local energy consumption is in mWh, and edge energy consumption is in Wh.

Network type	Scheme	$N_{MD}=40$		$N_{MD}=100$		$N_{MD}=160$	
		Local	Edge	Local	Edge	Local	Edge
Communication-intensive	Random	0.280	24.6	0.231	28.1	0.232	31.0
	Max SINR	0.172	19.5	0.128	22.4	0.128	25.2
	Max Compute	0.184	27.0	0.260	29.0	0.303	30.8
	Combined	0.177	23.6	0.183	26.4	0.211	28.7
	Proposed	<u>0.062</u>	8.42	<u>0.061</u>	8.97	<u>0.077</u>	9.44
Computation-intensive	Random	0.311	132	0.361	138	0.441	141
	Max SINR	0.301	126	0.324	149	0.365	182
	Max Compute	0.338	131	0.275	167	0.272	199
	Combined	0.315	109	0.303	138	0.332	166
	Proposed	<u>0.129</u>	89.9	<u>0.182</u>	94.8	<u>0.241</u>	100

work environments.

6.2.2 Energy Analysis

Now, we analyze the energy consumption results of the proposed scheme and the baseline schemes. The energy consumption per task under different network scenarios is shown in Table 5. The values indicate that our method achieves the lowest local energy consumption per task for both the communication-intensive network and computation-intensive network. In each network environment, our method consumed up to 64.0% and 57.1% less energy respectively compared to the best performing baseline model. The remarkable energy conservation performance while achieving low latency lies in the strategic offloading policy. As for the communication-intensive networks, since tasks impose high communication load, increasing the local computation ratio proves to be a viable solution. Therefore, the proposed scheme achieves an outstanding performance by modulating its offloading ratio accordingly. Conversely, in computation-intensive networks, where tasks have high computation load with relatively low communication load, increasing the offloading ratio could lead to better performance in both energy conservation and latency. Hence, the proposed method achieves the best performance by adaptively regulating its offloading ratio.

6.2.3 Pareto Graph Analysis

From Table 5, we analyzed how offloading ratio could effect the latency and the energy conservation performance. This leads to a question: *Could the baseline schemes outperform the proposed scheme if they increase their local computation ratio?* To answer this question, we plot a Pareto efficiency graph of the reciprocals of latency and energy consumption of the models. Pareto efficiency graph illustrates a trade-off relationship between two or more values. We compare the schemes' performance by examining their locations on the Pareto graph. Since better latency and energy consumption leads to larger reciprocals of their values, if the proposed scheme is located at the upper right of the baseline schemes, this indicates that the proposed scheme excels over the baselines in both latency and energy consumption. Additionally, if the proposed scheme surpasses the baseline in all axes, it indicates that the proposed scheme Pareto-dominates the baseline, signifying its superiority in all aspects.

To evaluate all possible cases of the baseline models, we simulate the network numerous times, while gradually

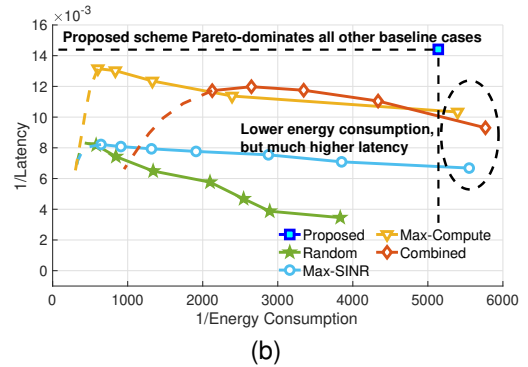
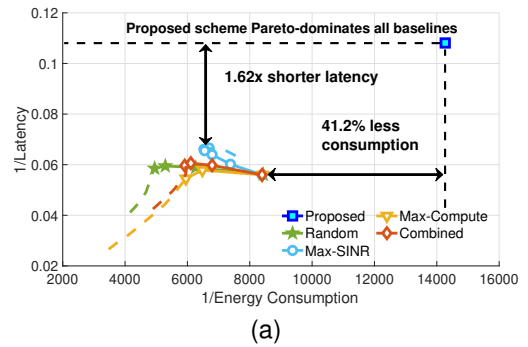


Fig. 7. Pareto efficiency graph of different networks with 80 MDs and 8 ESs, as ϵ ranges from 0.0 to 1.0: (a) Network with high communication load; (c) Network with high computational load.

increasing the offloading ratio ϵ from 0.0 to 1.0, with an increment of 0.1. As for the proposed model, we used $\alpha = 1$. As can be observed in Fig. 7a, in a system with heavy communication load, the proposed scheme's performance surpasses other baseline schemes in both latency and energy efficiency. In other words, our scheme Pareto-dominates all baseline schemes. More specifically, the proposed scheme achieved up to 1.62 times shorter latency compared to the best performing baseline models, while simultaneously consuming 41.2% less energy. The result indicates that the baseline schemes cannot outperform the proposed scheme, regardless of the offloading ratio. In Fig. 7b, some baseline schemes outperformed our scheme in terms of energy efficiency. However, our scheme still outperformed the baseline in latency, achieving up to 2.16 times shorter latency while using at most 10.9% more energy. We also remark that the proposed scheme can also achieve such good energy consumption by increasing α .

We note that in Fig. 7, we only emphasized the points of the agent performance that is Pareto-efficient, i.e., we only dramatized the best performances of each agent. The dashed line segments are affected by other factors such as task overload delay, but is negligible since the change of offloading ratio leads to better performance of both aspects of latency and energy efficiency.

6.2.4 Effects of unit-changing parameter α

In our problem formulation, we introduced a new variable α that balances MD's energy consumption and latency. Using α as a unit conversion parameter, we were able to jointly optimize energy usage and system latency. We now

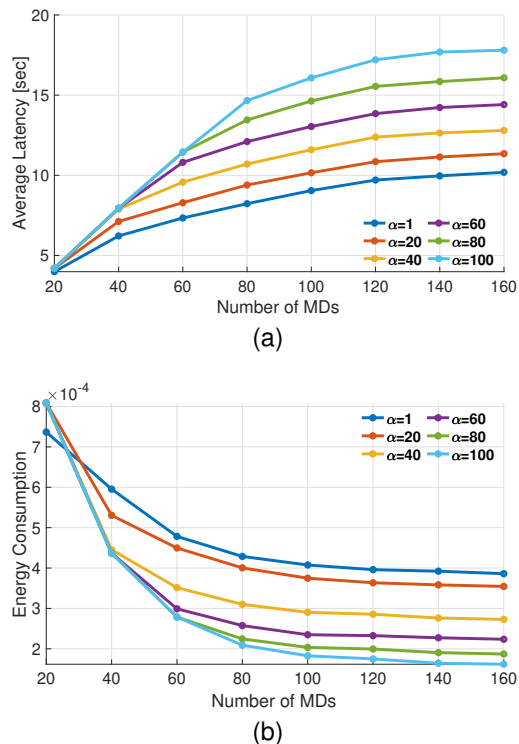


Fig. 8. Average latency and energy consumption of the network for various α ($N_{ES} = 4$): (a) Average latency for different α values. Latency rises with an increase of α due to the escalation of local computation; (b) Local energy consumption for different α values. Energy consumption decreases as α rises, due to the increase of local computation.

investigate the influence of α on the system's latency and energy consumption.

α is a weight that is multiplied to the energy penalty term of a device. The effect that the leftover energy has on the problem will increase as α increases. More intuitively, the proposed scheme will choose to compute on an edge device more often when α is large, in order to preserve energy.

The effect of α on the system latency is depicted in Fig. 8a. As predicted, the lowest latency is achieved when α is at its minimum. In networks with small number of users, the effects of α is not as severe as in networks with large number of users, as can be seen from the small gap between the latency. This is because the users experience sufficient amount of communication and computational resources when N_{MD} is small. Hence, the latency discrepancy between the systems is marginal when N_{MD} is small, and the gap grows as the number of MDs increases. Figure 8b visualizes the relationship between the number of MDs and the local energy consumption. Since higher value of α decreases the number of local computations, energy consumption naturally decreases as α increases.

In both of the figures of Fig. 8, the inclination of the graphs tend to converge after a certain number of users. The reason can be found from the convergence of the offloading ratio. As the number of MDs increases, the saturation rate of the ESs rises as there are more tasks to compute. But if the number of MDs is sufficiently large, the advantages of edge computing diminishes, as edge computing experiences bigger latency due to the overload of ES computation.

Therefore, the offloading ratio converges for large MDs, leading to a saturation of both the average latency and energy consumption of each MD.

7 CONCLUSION

This paper investigates AI-native MEC systems consisting of energy constrained users, and design a problem to optimize both the system latency and the user energy usage. Due to the coupled variables, the problem is decomposed into N_{ES} sub-problems, which is solved to provide an optimal solution. Through simulations, we show that the proposed scheme outperforms other baseline methods in terms of latency and energy usage. Our simulation results illustrate the relationship between the task loads of the MEC network, offloading policy and the energy usage, giving valuable insights on the optimal offloading and resource allocation methods. As a result, our method achieved a latency improvement of 1.62 times while reducing the energy consumption by 41.2%. Our best experiment in latency reduction exhibited a decrease in latency by 5.29 times. Also, the best experiment in energy consumption reduced energy consumption by up to 64.0%.

Although our method can cope with many types of network scenario in the long term, the optimization of users with high mobility still remains unsolved. Mobile device users in particular, may have high mobility which could be put into consideration in order to better optimize the offloading policy and tackle the handover problems between the ESs. In future works, minimizing energy usage, latency and the number of handovers between ESs in such scenarios by jointly optimizing resource allocation and user association could provide promising results.

REFERENCES

- [1] F. Chai, Q. Zhang, H. Yao, X. Xin, R. Gao, and M. Guizani, "Joint multi-task offloading and resource allocation for mobile edge computing systems in satellite iot," *IEEE Trans. Veh. Technol.*, vol. 72, no. 6, pp. 7783–7795, 2023.
- [2] H. Jiang, X. Dai, Z. Xiao, and A. Iyengar, "Joint task offloading and resource allocation for energy-constrained mobile edge computing," *IEEE Trans. Mobile Comput.*, vol. 22, no. 7, pp. 4000–4015, 2023.
- [3] A. Mohajer, M. Sam Daliri, A. Mirzaei, A. Ziaeddini, M. Nabipour, and M. Bavaghar, "Heterogeneous computational resource allocation for noma: Toward green mobile edge-computing systems," *IEEE Trans. Serv. Comput.*, vol. 16, no. 2, pp. 1225–1238, 2023.
- [4] L. T. Hoang, C. T. Nguyen, and A. T. Pham, "Deep reinforcement learning-based online resource management for uav-assisted edge computing with dual connectivity," *IEEE/ACM Trans. Networking*, pp. 1–16, 2023.
- [5] C. Deng, X. Fang, and X. Wang, "Uav-enabled mobile-edge computing for ai applications: Joint model decision, resource allocation, and trajectory optimization," *IEEE Internet Things J.*, vol. 10, no. 7, pp. 5662–5675, 2023.
- [6] W. He, Y. Zhang, Y. Huang, D. He, Y. Xu, Y. Guan, and W. Zhang, "Integrated resource allocation and task scheduling for full-duplex mobile edge computing," *IEEE Trans. Veh. Technol.*, vol. 71, no. 6, pp. 6488–6502, 2022.
- [7] T. Bahreini, H. Badri, and D. Grosu, "Mechanisms for resource allocation and pricing in mobile edge computing systems," *IEEE Trans. Parallel Distrib. Syst.*, vol. 33, no. 3, pp. 667–682, 2022.
- [8] X. Zhong, X. Wang, T. Yang, Y. Yang, Y. Qin, and X. Ma, "Potam: A parallel optimal task allocation mechanism for large-scale delay sensitive mobile edge computing," *IEEE Trans. Commun.*, vol. 70, no. 4, pp. 2499–2517, 2022.

- [9] Y. Liu, J. Yan, and X. Zhao, "Deep reinforcement learning based latency minimization for mobile edge computing with virtualization in maritime uav communication network," *IEEE Trans. Veh. Technol.*, vol. 71, no. 4, pp. 4225–4236, 2022.
- [10] Y. Chen, Z. Liu, Y. Zhang, Y. Wu, X. Chen, and L. Zhao, "Deep reinforcement learning-based dynamic resource management for mobile edge computing in industrial internet of things," *IEEE Trans. Ind. Informat.*, vol. 17, no. 7, pp. 4925–4934, 2021.
- [11] M. Zhao, J.-J. Yu, W.-T. Li, D. Liu, S. Yao, W. Feng, C. She, and T. Q. S. Quek, "Energy-aware task offloading and resource allocation for time-sensitive services in mobile edge computing systems," *IEEE Trans. Veh. Technol.*, vol. 70, no. 10, pp. 10925–10940, 2021.
- [12] J. Feng, Q. Pei, F. R. Yu, X. Chu, J. Du, and L. Zhu, "Dynamic network slicing and resource allocation in mobile edge computing systems," *IEEE Trans. Veh. Technol.*, vol. 69, no. 7, pp. 7863–7878, 2020.
- [13] Q. Ye, B. Rong, Y. Chen, M. Al-Shalash, C. Caramanis, and J. G. Andrews, "User association for load balancing in heterogeneous cellular networks," *IEEE Trans. Wireless Commun.*, vol. 12, no. 6, pp. 2706–2716, 2013.
- [14] P. Wang, Z. Zheng, B. Di, and L. Song, "Hetmec: Latency-optimal task assignment and resource allocation for heterogeneous multi-layer mobile edge computing," *IEEE Trans. Wireless Commun.*, vol. 18, no. 10, pp. 4942–4956, 2019.
- [15] J. Jang and H. J. Yang, " α -fairness-maximizing user association in energy-constrained small cell networks," *IEEE Trans. Wireless Commun.*, vol. 21, no. 9, pp. 7443–7459, 2022.
- [16] A. Khalili, S. Akhlaghi, H. Tabassum, and D. W. K. Ng, "Joint user association and resource allocation in the uplink of heterogeneous networks," *IEEE Commun. Lett.*, vol. 9, no. 6, pp. 804–808, 2020.
- [17] N. Trabelsi, C. S. Chen, R. El Azouzi, L. Roullet, and E. Altman, "User association and resource allocation optimization in lte cellular networks," *IEEE Trans. Netw. Service Manag.*, vol. 14, no. 2, pp. 429–440, 2017.
- [18] N. Zhao, Y.-C. Liang, D. Niyato, Y. Pei, M. Wu, and Y. Jiang, "Deep reinforcement learning for user association and resource allocation in heterogeneous cellular networks," *IEEE Trans. Wireless Commun.*, vol. 18, no. 11, pp. 5141–5152, 2019.
- [19] S. K. Singh, V. S. Borkar, and G. S. Kasbekar, "User association in dense mmwave networks as restless bandits," *IEEE Trans. Veh. Technol.*, vol. 71, no. 7, pp. 7919–7929, 2022.
- [20] X. Zhang, Z. Zhang, and L. Yang, "Learning-based resource allocation in heterogeneous ultradense network," *IEEE Internet Things J.*, vol. 9, no. 20, pp. 20229–20242, 2022.
- [21] K. Shen and W. Yu, "Distributed pricing-based user association for downlink heterogeneous cellular networks," *IEEE J. Select. Areas Commun.*, vol. 32, no. 6, pp. 1100–1113, 2014.
- [22] Q. Han, B. Yang, G. Miao, C. Chen, X. Wang, and X. Guan, "Backhaul-aware user association and resource allocation for energy-constrained hetnets," *IEEE Trans. Veh. Technol.*, vol. 66, no. 1, pp. 580–593, 2017.
- [23] M. Chen and Y. Hao, "Task offloading for mobile edge computing in software defined ultra-dense network," *IEEE J. Select. Areas Commun.*, vol. 36, no. 3, pp. 587–597, 2018.
- [24] M. Li, N. Cheng, J. Gao, Y. Wang, L. Zhao, and X. Shen, "Energy-efficient uav-assisted mobile edge computing: Resource allocation and trajectory optimization," *IEEE Trans. Veh. Technol.*, vol. 69, no. 3, pp. 3424–3438, 2020.
- [25] J. Feng, F. R. Yu, Q. Pei, J. Du, and L. Zhu, "Joint optimization of radio and computational resources allocation in blockchain-enabled mobile edge computing systems," *IEEE Trans. Wireless Commun.*, vol. 19, no. 6, pp. 4321–4334, 2020.
- [26] H. Xu, W. Huang, Y. Zhou, D. Yang, M. Li, and Z. Han, "Edge computing resource allocation for unmanned aerial vehicle assisted mobile network with blockchain applications," *IEEE Trans. Wireless Commun.*, vol. 20, no. 5, pp. 3107–3121, 2021.
- [27] J. Zhao, Q. Li, Y. Gong, and K. Zhang, "Computation offloading and resource allocation for cloud assisted mobile edge computing in vehicular networks," *IEEE Trans. Veh. Technol.*, vol. 68, no. 8, pp. 7944–7956, 2019.
- [28] W. Wu, F. Zhou, R. Q. Hu, and B. Wang, "Energy-efficient resource allocation for secure noma-enabled mobile edge computing networks," *IEEE Trans. Commun.*, vol. 68, no. 1, pp. 493–505, 2020.
- [29] Y. Deng, Z. Chen, X. Yao, S. Hassan, and A. M. A. Ibrahim, "Parallel offloading in green and sustainable mobile edge computing for delay-constrained iot system," *IEEE Trans. Veh. Technol.*, vol. 68, no. 12, pp. 12202–12214, 2019.
- [30] Q. Zhang, L. Gui, F. Hou, J. Chen, S. Zhu, and F. Tian, "Dynamic task offloading and resource allocation for mobile-edge computing in dense cloud ran," *IEEE Internet Things J.*, vol. 7, no. 4, pp. 3282–3299, 2020.
- [31] L. Huang, S. Bi, and Y.-J. A. Zhang, "Deep reinforcement learning for online computation offloading in wireless powered mobile-edge computing networks," *IEEE Trans. Mobile Comput.*, vol. 19, no. 11, pp. 2581–2593, 2020.
- [32] M. Tang and V. W. Wong, "Deep reinforcement learning for task offloading in mobile edge computing systems," *IEEE Trans. Mobile Comput.*, vol. 21, no. 6, pp. 1985–1997, 2022.
- [33] N. Kiran, C. Pan, S. Wang, and C. Yin, "Joint resource allocation and computation offloading in mobile edge computing for sdn based wireless networks," *J. Commun. Netw.*, vol. 22, no. 1, pp. 1–11, 2020.
- [34] S. Wang, M. Chen, X. Liu, C. Yin, S. Cui, and H. Vincent Poor, "A machine learning approach for task and resource allocation in mobile-edge computing-based networks," *IEEE Internet Things J.*, vol. 8, no. 3, pp. 1358–1372, 2021.
- [35] J. Feng, F. Richard Yu, Q. Pei, X. Chu, J. Du, and L. Zhu, "Cooperative computation offloading and resource allocation for blockchain-enabled mobile-edge computing: A deep reinforcement learning approach," *IEEE Internet Things J.*, vol. 7, no. 7, pp. 6214–6228, 2020.
- [36] S. Nath, Y. Li, J. Wu, and P. Fan, "Multi-user multi-channel computation offloading and resource allocation for mobile edge computing," in *ICC 2020 - 2020 IEEE International Conference on Communications (ICC)*, 2020, pp. 1–6.
- [37] K. Wang, D. Niyato, W. Chen, and A. Nallanathan, "Task-oriented delay-aware multi-tier computing in cell-free massive mimo systems," *IEEE J. Select. Areas Commun.*, vol. 41, no. 7, pp. 2000–2012, 2023.
- [38] 3GPP, "Scenarios and requirements for small cell enhancements for E-UTRA and E-UTRAN," 3rd Generation Partnership Project (3GPP), Technical Report (TR) 36.932, 07 2018, version 15.0.0.
- [39] V. A. Korthikanti, J. Casper, S. Lym, L. McAfee, M. Andersch, M. Shoeybi, and B. Catanzaro, "Reducing activation recomputation in large transformer models," *Proceedings of Machine Learning and Systems*, vol. 5, 2023.
- [40] 3GPP, "NR; Physical layer procedures for data," 3rd Generation Partnership Project (3GPP), TS 38.214, Jun. 2021.
- [41] —, "Small cell enhancements for E-UTRA and E-UTRAN - physical layer aspects," 3rd Generation Partnership Project (3GPP), TR 36.872, Dec. 2013.
- [42] T. Liu, S. Ni, X. Li, Y. Zhu, L. Kong, and Y. Yang, "Deep reinforcement learning based approach for online service placement and computation resource allocation in edge computing," *IEEE Trans. Mobile Comput.*, vol. 22, no. 7, pp. 3870–3881, 2023.
- [43] X. Ma, A. Zhou, S. Zhang, Q. Li, A. X. Liu, and S. Wang, "Dynamic task scheduling in cloud-assisted mobile edge computing," *IEEE Trans. Mobile Comput.*, vol. 22, no. 4, pp. 2116–2130, 2023.

Age-of-Information-Aware Distributed Task Offloading and Resource Allocation in Mobile Edge Computing Networks

Minwoo Kim, Jonggyu Jang, *Member, IEEE*, Youngchol Choi, and Hyun Jong Yang, *Member, IEEE*

APPENDIX A

OPTIMAL SOLUTION OF COMMUNICATION / COMPUTATION RESOURCE ALLOCATION

A.1 Optimal Solution of Communication Resource Allocation

We first relax problem \mathcal{P}_1 by dividing it into N_{ES} sub-problems, each problem corresponding to an ES, where

$$\sum_{i \in \mathcal{M}} \sum_{j \in \mathcal{E}} (D_{\text{cm},ij} + D_{\text{ES},i}) x_{ij} + \sum_{i \in \mathcal{M}} \left(1 - \sum_{j \in \mathcal{E}} x_{ij} \right) \left(D_{\text{MD},i} + \alpha \frac{G_i}{B_i} \right) \quad (\text{S1})$$

$$= \sum_{j \in \mathcal{E}} \sum_{i \in \mathcal{M}_j} (D_{\text{cm},ij} + D_{\text{ES},i}) + \sum_{i \in \mathcal{M}} \left(1 - \sum_{j \in \mathcal{E}} x_{ij} \right) \left(D_{\text{MD},i} + \alpha \frac{G_i}{B_i} \right) \quad (\text{S2})$$

Here, \mathcal{M}_j is a subset of \mathcal{M} such that $\mathcal{M}_j = \{i \in \mathcal{M} | x_{ij} = 1\}$. In equation (S2), we select x_{ij} that belongs in the set \mathcal{M}_j . Hence, the terms behind, which describes the latency and the cost occurring when we compute locally, can be ignored when considering the users from set \mathcal{M}_j . In other words, we're looking at the cases of i such that $x_{ij} = 1$.

As mentioned above, ignoring the terms behind, we can choose one of N_{ES} sub-problems from equation (S2). Using the modified objective function (S2), we can formulate the Lagrangian as

$$\mathcal{L}_1 = \sum_{i \in \mathcal{M}_j} (D_{\text{cm},i} + D_{\text{ES},i}) + \lambda^{(1)} \left(\sum_{i \in \mathcal{M}_j} y_{ij} - 1 \right) + \lambda^{(2)} \sum_{i \in \mathcal{M}_j} (z_{ij} - 1) - \sum_{i \in \mathcal{M}_j} (\lambda_i^{(3)} y_{ij} + \lambda_i^{(4)} z_{ij}). \quad (\text{S3})$$

From the Lagrangian (S3), we derive the KKT conditions of the problem as follows:

$$\left\{ \begin{array}{l} \frac{\partial \mathcal{L}_1}{\partial y_{ij}} = -\frac{d_i R_{ij}}{(R_{ij} y_{ij})^2} + \lambda^{(1)} - \lambda_i^{(3)} = 0 \end{array} \right. \quad (\text{S4a})$$

$$\left\{ \begin{array}{l} \frac{\partial \mathcal{L}_1}{\partial z_{ij}} = -\frac{f_i F_{\text{ES},j} Z_{\text{ES},j}}{(F_{\text{ES},j} Z_{\text{ES},j} z_{e_a})^2} \rho + \lambda^{(1)} - \lambda_i^{(3)} = 0 \end{array} \right. \quad (\text{S4b})$$

$$\left\{ \begin{array}{l} \lambda^{(1)} \left(\sum_{i \in \mathcal{M}_j} y_{ij} - 1 \right) = 0 \end{array} \right. \quad (\text{S4c})$$

$$\left\{ \begin{array}{l} \lambda^{(2)} \left(\sum_{i \in \mathcal{M}_j} z_{ij} - 1 \right) = 0 \end{array} \right. \quad (\text{S4d})$$

$$\left\{ \begin{array}{l} \lambda_i^{(3)} y_{ij} = 0 \end{array} \right. \quad (\text{S4e})$$

$$\left\{ \begin{array}{l} \lambda_i^{(4)} z_{ij} = 0 \end{array} \right. \quad (\text{S4f})$$

$$\left\{ \begin{array}{l} \lambda^{(1)} \geq 0 \end{array} \right. \quad (\text{S4g})$$

$$\left\{ \begin{array}{l} \lambda_i^{(3)} \geq 0, \lambda_i^{(4)} \geq 0, \lambda_i^{(2)} \geq 0 \forall i \in \mathcal{M}_j. \end{array} \right. \quad (\text{S4h})$$

From condition (S4a), we obtain a solution of y_{ij} , consisting of the Lagrangian multipliers $\lambda^{(1)}$ and $\lambda_i^{(3)}$. We divide the cases of possible y_{ij} according to the values of $\lambda^{(1)}$, and examine the cases to solve for the optimal y_{ij} .

1) *Case 1* ($\lambda^{(1)} = 0$; *Invalid Case*): In this case,

$$y_{ij} = \left(\sqrt{\frac{d_i R_{ij}}{-\lambda_i^{(3)}}} \right) / R_{ij}. \quad (\text{S5})$$

From equation (S5) and condition (S4h), there exists no feasible solution y_{ij} .

2) *Case 2* ($\lambda^{(1)} > 0$; *Valid Case*): In this case, we have

$$y_{ij} = \left(\sqrt{\frac{d_i R_{ij}}{\lambda^{(1)} - \lambda_i^{(3)}}} \right) / R_{ij}. \quad (\text{S6})$$

Because $y_{ij} > 0$, $\lambda_i^{(3)} = 0$ by condition (S4e). y_{ij} has a feasible solution in this case, and $y_{ij} = \left(\sqrt{\frac{d_i R_{ij}}{\lambda^{(1)}}} \right) / R_{ij}$.

Next, to solve for $\lambda^{(1)}$, we use the condition of y_{ij} , i.e., $\sum_{i \in \mathcal{M}_j} y_{ij} - 1 = 0$. Then, we have

$$\sum_{i \in \mathcal{M}_j} y_{ij} = \sum_{i \in \mathcal{M}_j} \left(\sqrt{\frac{1}{\lambda^{(1)}}} \sqrt{\frac{d_i}{R_{ij}}} \right) \quad (\text{S7})$$

$$= \sqrt{\frac{1}{\lambda^{(1)}}} \sum_{i \in \mathcal{M}_j} \sqrt{\frac{d_i}{R_{ij}}} = 1. \quad (\text{S8})$$

Therefore,

$$\lambda^{(1)} = \left(\sum_{i \in \mathcal{M}_j} \sqrt{\frac{d_i}{R_{ij}}} \right)^2. \quad (\text{S9})$$

Inserting the value above to equation (S6), we obtain the optimal y_{ij} as follows:

$$y_{ij} = \left(\sqrt{d_i / R_{ij}} \right) / \left(\sum_{k \in \mathcal{M}_j} \sqrt{d_k / R_{kj}} \right) \quad (\text{S10})$$

$$= \left(\sqrt{d_i / R_{ij}} \right) / \left(\sum_{k \in \mathcal{M}} \sqrt{d_k / R_{kj}} x_{ij} \right). \quad (\text{S11})$$

A.2 Optimal Solution of Computation

We use the Lagrangian (S3) derived from Appendix A.1. After solving for z_{e_a} , we divide the cases of $\lambda^{(1)}$.

1) *Case 1* ($\lambda^{(1)} = 0$; *Invalid Case*): In this case,

$$z_{ij} = \left(\sqrt{\frac{f_i F_{\text{ES},j} Z_{\text{ES},j} \rho}{-\lambda_i^{(3)}}} \right) / F_{\text{ES},j} Z_{\text{ES},j}. \quad (\text{S12})$$

From equation (S12) and condition (S4h), there exists no feasible solution z_{ij} , as z_{ij} either becomes imaginary or diverges.

2) *Case 2* ($\lambda^{(1)} > 0$; *Valid Case*): As for this case, z_{ij} is expressed as follows:

$$z_{ij} = \left(\sqrt{\frac{f_i F_{\text{ES},j} Z_{\text{ES},j} \rho}{\lambda^{(1)}}} \right) / F_{\text{ES},j} Z_{\text{ES},j}. \quad (\text{S13})$$

Solving equation (S13) gives $z_{ij} > 0$, which leads to $\lambda_i^{(3)} = 0$ by condition (S4f). No contradiction occurs in this case, and

$$z_{ij} = \left(\sqrt{\frac{f_i F_{\text{ES},j} Z_{\text{ES},j} \rho}{\lambda^{(1)}}} \right) / F_{\text{ES},j} Z_{\text{ES},j}.$$

Next, we use the resource allocation condition of z_{ij} , i.e., $\sum_{i \in \mathcal{M}_j} z_{ij} - 1 = 0$. Then, we have the following condition:

$$\sum_{i \in \mathcal{M}_j} z_{ij} = \sum_{i \in \mathcal{M}_j} \left(\sqrt{\frac{1}{\lambda^{(1)}}} \sqrt{\frac{f_i \rho}{F_{ES,j} Z_{ES,j}}} \right) \quad (S14)$$

$$= \sqrt{\frac{1}{\lambda^{(1)}}} \sum_{i \in \mathcal{M}_j} \sqrt{\frac{f_i \rho}{F_{ES,j} Z_{ES,j}}} = 1. \quad (S15)$$

Therefore,

$$\lambda^{(1)} = \left(\sum_{i \in \mathcal{M}_j} \sqrt{\frac{f_i \rho}{F_{ES,j} Z_{ES,j}}} \right)^2. \quad (S16)$$

Inserting the value above to equation (S6), we can obtain the optimal y_{ij} as follows:

$$\begin{aligned} y_{ij} &= \left(\sqrt{f_i \rho / F_{ES,j} Z_{ES,j}} \right) / \left(\sum_{k \in \mathcal{M}_j} \sqrt{f_k / F_{ES,j} Z_{ES,j}} \right) \\ &= \left(\sqrt{f_i \rho / F_{ES,j} Z_{ES,j}} \right) / \left(\sum_{k \in \mathcal{M}} \sqrt{f_k / F_{ES,j} Z_{ES,j} x_{ij}} \right). \end{aligned} \quad (S17)$$

APPENDIX B PROOF OF THEOREM 1

In the Lagrangian duality, the weak duality holds for all feasible solutions, i.e., $d^* \leq f^*$ (minimization problem), where d^* and f^* denote the optimal dual function and optimal primal function, respectively. However, in the proposed method, the variable \mathbf{X} recovered by the dual approach cannot meet the auxiliary constraints (\mathcal{P}_6d) and (\mathcal{P}_6e). Thus, there is a gap between the objective function of the primal problem \mathcal{P}_6 and the actual delay corresponding to \mathbf{X} , which are denoted as:

- The objective function of the primal problem \mathcal{P}_6 : $\sum_{j \in \mathcal{E}} (a_j + b_j) + \sum_{i \in \mathcal{M}} \sum_{j \in \mathcal{E}} c_{ij} x_{ij}$.
- Actual delay with penalized energy consumption corresponding to \mathbf{X} :

$$\begin{aligned} &\sum_{j \in \mathcal{E}} \left(\sum_{i \in \mathcal{M}} \sqrt{D_{ES(s),ij} x_{ij}} \right)^2 + \sum_{j \in \mathcal{E}} \left(\sum_{i \in \mathcal{M}} \sqrt{D_{cm,ij} x_{ij}} \right)^2 \\ &+ \sum_{i \in \mathcal{M}} \sum_{j \in \mathcal{E}} c_{ij} x_{ij}. \end{aligned}$$

Here, we first show that the weak duality still holds for the actual delay if we use this instead of the objective function of the problem \mathcal{P}_6 .

B.1 Conservation of the Weak Duality Condition

Denoting the solution we obtained from Lagrangian dual problem \mathcal{P}_7 as $\boldsymbol{\mu}^*$ and $\boldsymbol{\nu}^*$, we can represent the maximum value of the Lagrangian dual function as $d^* = g(\boldsymbol{\mu}^*, \boldsymbol{\nu}^*)$. Here, we denote the global optimal solution minimizing the

objective function in \mathcal{P}_5 as \hat{f}^* . Denoting the solution we obtained as \hat{f} , the following inequality holds:

$$\begin{aligned} d^* &= \max_{\boldsymbol{\mu}, \boldsymbol{\nu}} \min_{\mathbf{a}, \mathbf{b}, \mathbf{X}} \mathcal{L}(\mathbf{a}, \mathbf{b}, \mathbf{X}, \boldsymbol{\mu}, \boldsymbol{\nu}) \\ &\leq \max_{\boldsymbol{\mu}, \boldsymbol{\nu}} \min_{\mathbf{a}, \mathbf{b}, \mathbf{X} \in \mathcal{F}} \mathcal{L}(\mathbf{a}, \mathbf{b}, \mathbf{X}, \boldsymbol{\mu}, \boldsymbol{\nu}) \\ &= \min_{\mathbf{a}, \mathbf{b}, \mathbf{X} \in \mathcal{F}} \sum_{j \in \mathcal{E}} \left(\sum_{i \in \mathcal{M}} \sqrt{D_{ES(s),ij} x_{ij}} \right)^2 \\ &\quad + \sum_{j \in \mathcal{E}} \left(\sum_{i \in \mathcal{M}} \sqrt{D_{cm,ij} x_{ij}} \right)^2 \\ &\quad + \sum_{i \in \mathcal{M}} \sum_{j \in \mathcal{E}} c_{ij} x_{ij} \\ &= \hat{f}^* \leq \hat{f}. \end{aligned} \quad (S18)$$

where \mathcal{F} denotes a space where the constraints (\mathcal{P}_6d) and (\mathcal{P}_6e) hold.

B.2 Duality Gap

In the previous section, we show that the weak duality condition still holds for the solution with recovered \mathbf{X} . Then, inspired by the inequality in (S18), we show the duality gap of the solution for recovered \mathbf{X} . Let us represent the solution \hat{f} as

$$\begin{aligned} \hat{f} &= \sum_{j \in \mathcal{E}} \left(\sum_{i \in \mathcal{M}} \sqrt{D_{ES(s),ij} x_{ij}} \right)^2 \\ &\quad + \sum_{j \in \mathcal{E}} \left(\sum_{i \in \mathcal{M}} \sqrt{D_{cm,ij} x_{ij}} \right)^2 + \sum_{i \in \mathcal{M}} \sum_{j \in \mathcal{E}} c_{ij} x_{ij} \quad (S19) \\ &= \sum_{j \in \mathcal{E}} (\sqrt{a_j} - \Delta_j^{(1)})^2 + \sum_{j \in \mathcal{E}} (\sqrt{b_j} - \Delta_j^{(2)})^2 + \sum_{i \in \mathcal{M}} \sum_{j \in \mathcal{E}} c_{ij} x_{ij}, \end{aligned}$$

where $\Delta_j^{(1)} = \sqrt{a_j} - (\sum_{i \in \mathcal{M}} \sqrt{D_{cm,ij} x_{kj}})$ and $\Delta_j^{(2)} = \sqrt{b_j} - (\sum_{i \in \mathcal{M}} \sqrt{D_{ES(s),ij} x_{ij}})$. Then, we have the optimality gap as below:

$$\hat{f} - \hat{f}^* \quad (S20)$$

$$\leq \hat{f} - d^* \quad (S21)$$

$$= \sum_{j \in \mathcal{E}} (\sqrt{a_j} - \Delta_j^{(1)})^2 + \sum_{j \in \mathcal{E}} (\sqrt{b_j} - \Delta_j^{(2)})^2 \quad (S22)$$

$$- \sum_{j \in \mathcal{E}} a_j - \sum_{j \in \mathcal{E}} b_j \quad (S23)$$

$$\leq \sum_{j \in \mathcal{E}} \left((\Delta_j^{(1)})^2 + (\Delta_j^{(2)})^2 - 2\sqrt{a_j} \Delta_j^{(1)} - 2\sqrt{b_j} \Delta_j^{(2)} \right).$$

Finally, we confirm that the optimality gap of the proposed scheme is bounded by $\mathcal{O} \left((\Delta_j^{(1)})^2 + (\Delta_j^{(2)})^2 \right)$.

APPENDIX C PROOF OF PROPOSITION 1

Here, we prove the convergence of the proposed scheme. Let us define the optimal solution to Problem \mathcal{P}_7 as $\boldsymbol{\mu}^*$ and $\boldsymbol{\nu}^*$.

To solve the problem \mathcal{P}_7 , we apply the sub-gradient ascent in (31), which is represented by

$$\begin{aligned}\boldsymbol{\mu}^{(t+1)} &= \boldsymbol{\mu}^{(t)} + \eta_1 \nabla_{\boldsymbol{\mu}} g(\boldsymbol{\mu}, \boldsymbol{\nu}), \forall t \in \{0, 1, \dots\} \\ \boldsymbol{\nu}^{(t+1)} &= \boldsymbol{\nu}^{(t)} + \eta_2 \nabla_{\boldsymbol{\nu}} g(\boldsymbol{\mu}, \boldsymbol{\nu}), \forall t \in \{0, 1, \dots\}.\end{aligned}\quad (\text{S24})$$

To show the convergence, we assume $\|\nabla_{\boldsymbol{\mu}} g(\boldsymbol{\mu}, \boldsymbol{\nu})\|_2 \leq \delta_1$, $\|\nabla_{\boldsymbol{\nu}} g(\boldsymbol{\mu}, \boldsymbol{\nu})\|_2 \leq \delta_1$, $\|\boldsymbol{\mu}^{(0)} - \boldsymbol{\mu}^*\|_2 \leq \delta_2$, and $\|\boldsymbol{\nu}^{(0)} - \boldsymbol{\nu}^*\|_2 \leq \delta_2$. For brevity of the notation, we denote $\nabla_{\boldsymbol{\mu}} g(\boldsymbol{\mu}, \boldsymbol{\nu})$ and $\nabla_{\boldsymbol{\nu}} g(\boldsymbol{\mu}, \boldsymbol{\nu})$ as $\Delta_{\boldsymbol{\mu}}$ and $\Delta_{\boldsymbol{\nu}}$, respectively. Then, we have

$$\begin{aligned}\|\boldsymbol{\mu}^{(t+1)} - \boldsymbol{\mu}^*\|_2 - \|\boldsymbol{\mu}^{(t)} - \boldsymbol{\mu}^*\|_2 \\ = \eta_1^2 \|\Delta_{\boldsymbol{\mu}}\|_2 - 2\eta_1 (\Delta_{\boldsymbol{\mu}})^{\text{T}} (\boldsymbol{\mu}^* - \boldsymbol{\mu}^{(t)})\end{aligned}\quad (\text{S25})$$

and

$$\begin{aligned}\|\boldsymbol{\nu}^{(t+1)} - \boldsymbol{\nu}^*\|_2 - \|\boldsymbol{\nu}^{(t)} - \boldsymbol{\nu}^*\|_2 \\ = \eta_2^2 \|\Delta_{\boldsymbol{\nu}}\|_2 - 2\eta_2 (\Delta_{\boldsymbol{\nu}})^{\text{T}} (\boldsymbol{\nu}^* - \boldsymbol{\nu}^{(t)}),\end{aligned}\quad (\text{S26})$$

where the inequality holds due to the convexity. Let us define $g_{\max, T} = \max_{t=1, \dots, T} g(\boldsymbol{\mu}, \boldsymbol{\nu})$. By combining the inequalities from $t = 0$ to T , we have

$$\begin{aligned}2(T+1)(g^* - g_{\max, T}) \\ \leq 2 \sum_{t=0}^T (g^* - g(\boldsymbol{\mu}, \boldsymbol{\nu})) \\ \leq 2 \sum_{t=0}^T \left((\nabla_{\boldsymbol{\mu}})^{\text{T}} (\boldsymbol{\mu}^* - \boldsymbol{\mu}^{(t)}) + (\nabla_{\boldsymbol{\nu}})^{\text{T}} (\boldsymbol{\nu}^* - \boldsymbol{\nu}^{(t)}) \right) \\ = \eta_1 \sum_{t=0}^T \|\Delta_{\boldsymbol{\mu}}\|_2 + \eta_2 \sum_{t=0}^T \|\Delta_{\boldsymbol{\nu}}\|_2 \\ + \frac{1}{\eta_1} \|\boldsymbol{\mu}^{(0)} - \boldsymbol{\mu}^*\|_2 - \frac{1}{\eta_1} \|\boldsymbol{\mu}^{(T+1)} - \boldsymbol{\mu}^*\|_2 \\ + \frac{1}{\eta_2} \|\boldsymbol{\nu}^{(0)} - \boldsymbol{\nu}^*\|_2 - \frac{1}{\eta_2} \|\boldsymbol{\nu}^{(T+1)} - \boldsymbol{\nu}^*\|_2 \\ \leq (\eta_1 + \eta_2)(T+1)\delta_1 + \left(\frac{1}{\eta_1} + \frac{1}{\eta_2} \right) \delta_2.\end{aligned}\quad (\text{S27})$$

Finally, the inequality in (S27) can be rewritten as

$$g^* - g_{\max, T} \leq \frac{(\eta_1 + \eta_2)\delta_1}{2} + \frac{\delta_2}{2(T+1)} \left(\frac{1}{\eta_1} + \frac{1}{\eta_2} \right). \quad (\text{S28})$$

By choosing $\eta_1 = \eta_2 = \sqrt{\frac{\delta_2}{(T+1)\delta_1}}$, the following condition holds: $g^* - g_{\max, T} \leq \epsilon$, where $\epsilon = \sqrt{\frac{\delta_1 \delta_2}{(T+1)}}$. Thus, for any $\epsilon > 0$, there exist η_1 , η_2 , and $T \in \mathcal{O}(\frac{1}{\epsilon^2})$ satisfying $g^* - g_{\max, T} \leq \epsilon$.

This figure "fig1.png" is available in "png" format from:

<http://arxiv.org/ps/2404.03154v1>